# MASSIVELY-PARALLEL SPECTRAL ELEMENT LARGE EDDY SIMULATION OF A RING-TYPE GAS TURBINE COMBUSTOR

A Thesis

by

JOSHUA LANE CAMP

Submitted to the Office of Graduate Studies of
Texas A&M University
in partial fulfillment of the requirements for the degree of

MASTER OF SCIENCE

May 2011

Major Subject: Mechanical Engineering

# MASSIVELY-PARALLEL SPECTRAL ELEMENT LARGE EDDY SIMULATION OF A RING-TYPE GAS TURBINE COMBUSTOR

A Thesis

by

JOSHUA LANE CAMP

Submitted to the Office of Graduate Studies of
Texas A&M University
in partial fulfillment of the requirements for the degree of

MASTER OF SCIENCE

Approved by:

| | |
|---|---|
| Chair of Committee, | Andrew Duggleby |
| Committee Members, | Theofanis Strouboulis |
| | Eric Petersen |
| Head of Department, | Dennis O'Neal |

May 2011

Major Subject: Mechanical Engineering

# ABSTRACT

Massively-parallel Spectral Element Large Eddy Simulation of a Ring-type Gas Turbine Combustor. (May 2011)

Joshua Lane Camp, B.S., Baylor University

Chair of Advisory Committee: Dr. Andrew Duggleby

The average and fluctuating components in a model ring-type gas turbine combustor are characterized using a Large Eddy Simulation at a Reynolds number of 11,000, based on the bulk velocity and the mean channel height. A spatial filter is applied to the incompressible Navier-Stokes equations, and a high pass filtered Smagorinsky model is used to model the sub-grid scales. Two cases are studied: one with only the swirler inlet active, and one with a single row of dilution jets activated, operating at a momentum flux ratio $J$ of 100. The goal of both of these studies is to validate the capabilities of the solver NEK5000 to resolve important flow features inherent to gas turbine combustors by comparing qualitatively to the work of Jakirlic. Both cases show strong evidence of the Precessing Vortex Core, an essential flow feature in gas turbine combustors. Each case captures other important flow characteristics, such as corner eddies, and in general predicts bulk flow movements well. However, the simulations performed quite poorly in terms of predicting turbulence shear stress quantities. Difficulties in properly emulating the turbulent velocity entering the combustor for the swirl, as well as mesh quality concerns, may have skewed the results. Overall, though small length scale quantities were not accurately captured, the large scale quantities were, and this stress test on the HPF LES model will be built upon in future work that looks at more complex combustors.

To my wife Kaleigh

# ACKNOWLEDGMENTS

I would first like to thank my parents, Barbara and Elmo, and my brothers, Ty and Chaise, for making me who I am today. You have given me the strength and the tools to succeed, and I owe a great deal to you. My advisor, Adnrew Duggleby, has taught me so much, and I look forward to the many new things I will learn and accomplish while studying under him. My labmates, both current and past, (Shriram, Markus, Michael, William, Pradeep, and Sebastian) have provided tremendous support both in terms of helping me understand key concepts or just being someone to bounce ideas off of. Some of my closest friends have been through this process with me, and I have appreciated the support I have been given. Finally, I would like to thank my loving wife Kaleigh. You have been there with me every step of the way and given me the love needed to get me through many hard nights of work. I love you, and you are the reason for all that I do.

# NOMENCLATURE

| | |
|---|---|
| $C_s$ | Smagorinsky Coefficient |
| $H$ | High Pass Filter Function |
| $P$ | Static Pressure |
| $P_o$ | Total Pressure, $P + \frac{\rho U^2}{2}$ |
| $Q_{comb}$ | Heat Input to the Combustor, via Fuel |
| $Re$ | Reynolds Number |
| $U$ | Absolute Velocity, $\sqrt{u_j u_j}$ |
| $U_\infty$ | Characteristic Velocity |
| $V$ | Volume |
| $W_{net}$ | Net Amount of Work Produced in a Cycle |
| $W_{turb}$ | Work Output of the Turbine |
| $\Delta$ | Filter Width |
| $\bar{S}_{ij}$ | Strain Rate Tensor on Filtered Velocity |
| $\eta_{th}$ | Thermal Efficiency, First Law Efficiency |
| $\nu$ | Kinematic Viscosity |
| $\nu_t$ | Eddy Viscosity |
| $\nu_t^{HPF}$ | High Pass Filter Eddy Viscosity |

| | |
|---|---|
| $\rho$ | Density |
| $\tau_{ij}$ | Sub Grid Stress Tensor |
| $u_j$ | Velocity Component |
| $w$ | Specific Work |
| CFD | Computational Fluid Dynamics |
| DNS | Direct Numerical Simulation |
| DOF | Degree of Freedom |
| FEM | Finite Element Method |
| GLL | Gauss-Lobatto-Legendre |
| GT | Gas Turbine |
| LES | Large Eddy Simulation |
| PVC | Precessing Vortex Core |
| RANS | Reynolds-Averaged Navier-Stokes |
| SEM | Spectral Element Method |

TABLE OF CONTENTS

# LIST OF TABLES

# LIST OF FIGURES

FIGURE Page

# CHAPTER I

## INTRODUCTION

Energy is an area of research that continues to garner a lot of attention from the scientific and engineering communities. Topics that fall under this category vary from general topics such as investigating renewable resources and reducing emission to specific ones such as improving gas mileage in consumer vehicles and creating faster commercial jets. While discovering new energy resources in itself is an important concept, the rate of energy consumption, or power, is perhaps equally important. Power generation is what drives the modern world. The improvements in electrical systems and transportation over the past century (and more) are all directly related to improvements in how we understand power.

In all power-generating devices, the goal is to take an energy source and convert it into a form that is useful (work) in an efficient manner. A wind turbine is an example of this. Wind turbines are found in places ranging from the open plains of Texas to the ocean. The working principle of these devices is to remove energy from the wind (from the movement of the air) by allowing it to flow over large blades. This creates a force on the blades that causes the rotor to spin. A similar example of this type of power generation machine is a hydroelectric dam. In this case, the potential energy from the height of the water is extracted. These machines are great concepts because of the fact that their energy sources are "free." In a general sense, there are no fuel costs associated with wind turbines or hydroelectric dams. The disadvantage for these systems is that they do not generate a lot of power, when normalized by their size, compared to other methods. This makes them unsuitable for applications

---

The journal model is *IEEE Transactions on Automatic Control*.

like cars or aircraft.

In order to create the required amount of power in smaller form factors, more dense forms of energy must be consumed. This principle is in use in reciprocating engines found in consumer vehicles. These work by adding fuel (such as gasoline) to air, compressing it, and then igniting the mixture. This ignition rapidly expands the piston, providing work at a high rate (high power) that allows the car to overcome friction and move forward. These engines, while being much smaller than wind turbines, can generate a large amount of power. The disadvantage is that the energy source consumed is not freely available like already flowing wind or water and may also not be easily renewed, such as fossil fuels. A heavy focus of research is in alternative fuels in an attempt to reduce the dependence on fossil fuels. However, it has been difficult thus far to find alternatives that provide as much energy density as fossil fuels.

Gas turbine engines are a further example of a machine that converts an energy source into useful work. However, the differentiating factor between gas turbines and reciprocating engines is power density. For a given volume, gas turbine engines can produce much more power than a typical reciprocating engine. Because of this, gas turbine engines will be extremely important machines to study while fossil fuels are still the world's primary energy source. The goal of this thesis work, then, is to perform a high end simulation on an integral component of the engine, the combustor, in the hopes of gaining information that will help improve designs of gas turbine engines. The following section explains the function of gas turbines in more detail.

## A. Overview and Operation of Gas Turbine Engines

Gas turbine engines (hereafter referred to as GT engines) are mainly used for two purposes: propulsion and power generation. GT engines used for propulsion, commonly known as jet engines, are found on both commercial airliners and military fighter jets. In jet engines, air is sucked into the engine by the fan, raised to a higher pressure in the compressor section, mixed with fuel and burned in the combustor, and sent through the turbine section to extract energy, and then accelerated through the nozzle to the atmosphere, providing thrust. The power generated in the turbine section is used to power the compressor section, as well as any onboard electrical systems. For jet engines, a balance must be sought between thrust and weight. A large engine can provide more thrust, but the engine will also be heavier and may not be suited for smaller aircraft, such as military jets. The operation of power generation GT engines is similar, except that the goal is to generate power through the turbine, not provide thrust. Any power that is not used to power the compressor is power gained. Typically, the leftover power would be spent providing torque to a generator, converting the generated power to electricity. Since these GT engines are on the ground, they can be scaled up to meet whatever the required power demands are.

Figure 1 shows an example of a jet engine, the Rolls-Royce BR710 Turbofan Engine. The major components, which are similar for both jet engines and power generation units, are labeled. These components are (1) the compressor, (2) the combustor, and (3) the turbine, and the following sections detail how these three components make the engine work as a whole.

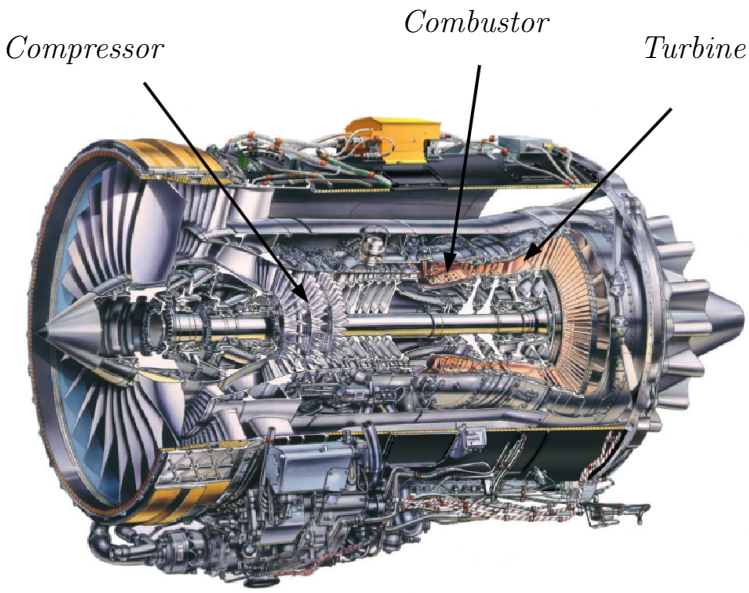


Fig. 1.: Example aircraft gas turbine engine. The Rolls Royce BR710 Turbofan Engine [1]. The major components and features are labeled.

## 1. Compressor

The main function of the compressor is to increase the total pressure of the working fluid (typically air). There are two types of compressors: axial compressors, and centrifugal compressors. The type typically found in GT engines are the axial kind. Axial compressors consist of a series of blade rows that alternative between stationary rows (stators) and rows that are attached to a rotating shaft (rotors). Typical pressure ratios (the ratio of the fluid pressure exiting the compressor to that entering) are between 15 and 30 [2]. Figure 2 shows a simple schematic of a single compressor stage, consisting of one stator and one rotor. Conservation of energy is the key to un-

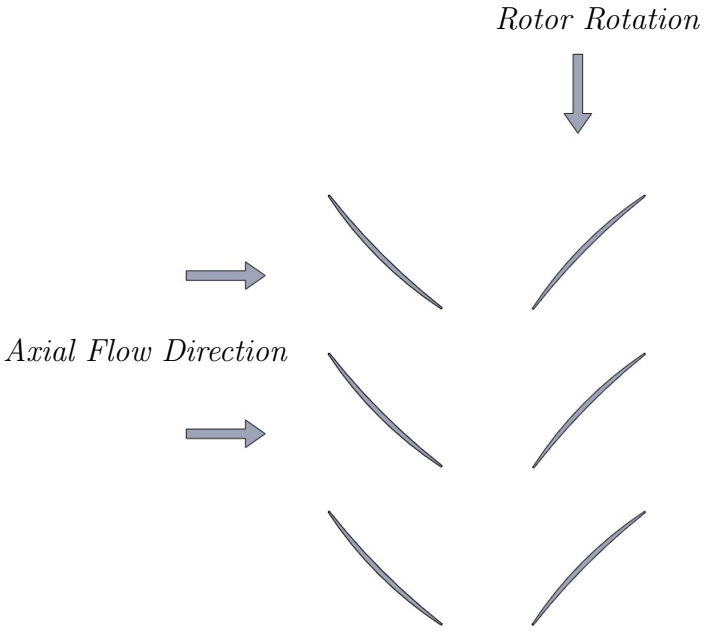


Fig. 2.: Flow diagram of compressor stage. The stator row (left) is followed immediately by the rotor row. The rotational energy of the rotor is imparted on the flowing air, which is responsible for increasing the total pressure

derstanding how a compressor stage elevates the total pressure of the air. Bernoulli's equation states that along streamlines and in the absence of any viscous forces, work interactions, or density changes, the total pressure, $P_o$ is constant, as seen in Equation 1.1,

$$P_i + \frac{\rho_i U_i^2}{2} = P_{o,i} = P_{o,e}, \tag{1.1}$$

where $P$ is the static pressure, $\rho$ is the density of the fluid, and $U$ is the magnitude of the velocity. The subscripts $i$ and $e$ represent the inlet and exit of a particular control volume. Although the flow in the compressor can not be assumed incompressible, the relationship between total and static pressure implied by the equation still holds true. Thus, in the stator flow, there is negligible change in total pressure, neglecting any friction effects. However, in the rotor row, the rotational energy of the blades is partially transferred to the air [2]. Equation 1.2 is a slightly modified version of Bernoulli's equation that incorporates the effects of energy transfer from an outside source,

$$P_{o,i} + \rho w = P_{o,e}, \tag{1.2}$$

where $w$ represents the portion of energy that is transferred from the rotor blade movement to the air. Thus, the total pressure of the air is increased when passing through the rotor.

The deflection angle, governed by the curvature of the blade, is a major factor in how much the pressure is increased in a given stage. A higher deflection angle leads to a larger increase. However, in any fluid flow, the natural tendency of the fluid is to flow from a high pressure zone to a low pressure alone. An example of this is seen everyday in the movement of weather systems. In a compressor, the desired direction of motion is contrary to this principle. Therefore, the pressure must be increased in stages, a little bit at a time. A sudden backflow of air, known as surge, can be

disastrous for the compressor blades, as these blades are not typically designed to withstand the high temperatures of the air-gas mixture present in the combustor. To prevent this, many more stages must be used in the compressor section than the turbine section, as seen in Figure 1. Once through the compressor, the air is at a much higher pressure and temperature, and it is ready to enter the combustor.

## 2. Combustor

The combustion section, or combustor, of a GT engine takes the high pressure air exiting the compressor and mixes it with fuel in the combustion chamber. This mixture is then ignited, releasing a large amount of energy in the process and greatly increasing the temperature of the flow. While combustors come in many different forms, there are two major types that are used. The annular can-type combustor consists of several combustor cans arranged in a ring. Each can is isolated from the others, and if there are $N$ different cans, there are $N$ different combustion processes. However, this type of design is typically only seen on older generation hardware. The other design is the ring-type annular combustor. Instead of several different cans, the entire ring is the combustor, with several different injection nozzles. Figure 3 shows two example mockups illustrating the fundamental differences.

Whether the combustor is a can-type or a ring-type, a typical combustor will have the same main features. Figure 4 shows a cutaway of a ring-type combustor, with the major parts labeled. Once the air exits from the last stage of the compressor, it enters the diffuser. The purpose of the diffuser is to route the air to both the combustor chamber and the secondary ducts, but more importantly, it slows the air down. Even though the compressor slows the air down some, it still comes into the combustor way too fast for the reaction flame inside the chamber to be stable. The portion that enters the chamber is drawn into a series of swirlers. The swirl nozzle

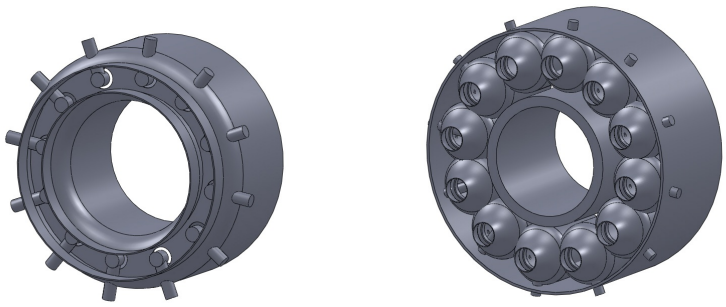

(a) Ring-type combustor (b) Can-type combustor

Fig. 3.: Comparison between ring-type and can-type combustor. The ring-type (left) is one integrated combustion ring, comprised of several segments fit together. The can-type contains several isolated combustion chambers.

shown in Figure 4 has several rectangular ducts that lie tangent to the nozzle. In this configuration, swirl is imparted on the flow naturally because of the tangential alignment of the ducts. Other swirl nozzles contain aerodynamically curved blades that are similar to the stator blades found in the compressor and turbine sections. In these configurations, instead of the air being drawn in the radial direction of the nozzle, the air is forced through the nozzle in the axial direction. The air flows around the blade, imparting swirl. In both cases, the fuel enters through the nozzle as well. The fuel is sent through a very thin ring in the nozzle, allowing it to exit as thin film. The thin film of fuel meets the highly swirling air, allowing them to thoroughly mix. The design of the swirl nozzle is a crucial to allowing efficient combustion. The better the fuel is mixed with the air, the cleaner and more complete the chemical reaction will be.

In order to keep the reaction flame contained inside the chamber, a portion of the

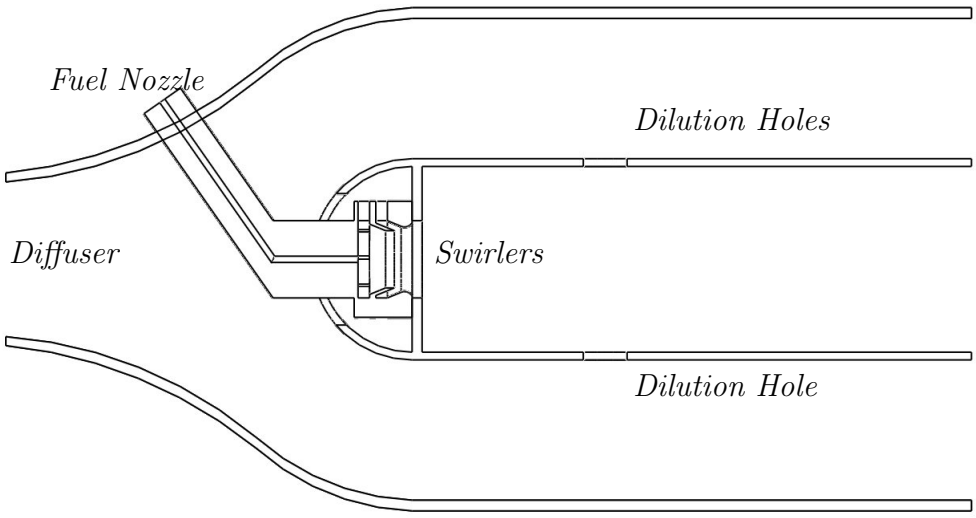


Fig. 4.: Cutaway of typical ring-type combustor. The major components are labeled. Compressed air at an elevated temperature enters from the left, where it decelerates in the diffuser. The air is split the core and to the secondary ducts. The core air is sent through swirlers, mixed with fuel coming from the nozzle, and ignited (ignition source not shown). A portion of the air enters the combustion chamber through the dilution holes at a high velocity, where it is used to help maintain the flame, while the rest is sent to the turbine blades for cooling. The combustion gases exit the chamber to the right, where the first turbine vane sits.

air that was sent to the secondary ducts enters the chamber through a series of dilution holes. The dilution flows causes the combustion gases to flow back on themselves, thus increasing mixing and keeping the flame from shooting through the turbine. It also cools the combustion gasses down some as it exits and enters turbine section. In addition, a portion of the secondary air enters the chamber through several small holes that lie perpendicular to the chamber wall. This air forms a thin layer of cooler air that lines the chamber walls, forming a boundary between the high temperature combustion gasses and the thin walls. This prevents the material in the chamber walls from melting. The rest of the secondary flow is sent to the turbine section, where it can used for cooling in the turbine blades and on the endwall.

The fuel-air mixture, now at a much higher temperature and pressure, next enters the turbine.

### 3. Turbine

The turbine section of the GT engine is the most essential part to design correctly. If the turbine section does not perform its function properly, then all of the work that was done upstream in the compressor and the combustor will go to waste. The working principle behind the operation of the gas turbine is the same as that for the compressor. However, in the turbine section, the high velocity, high pressure gas mixture is the source of energy, and the turbine blades are there to convert some of that energy to mechanical work. This is the equivalent of taking the work term, $w$, and moving it to the right hand side of Equation 1.2. Figure 5 shows a typical turbine stage.

The turbine section contains far fewer stages than the compressor, and the turbine blades themselves feature more extreme deflection angles than their compressor counterparts. This is due to the favorable pressure gradient present in the turbine

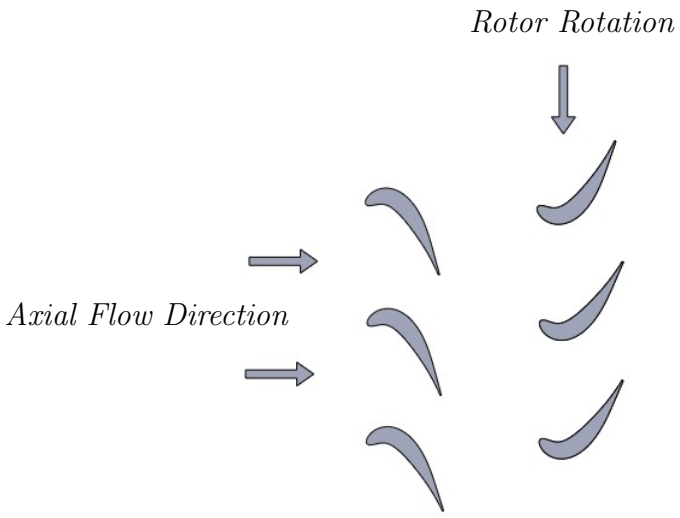


Fig. 5.: Flow diagram of turbine stage. The stator row (left) is followed immediately by the rotor row. The high velocity flow creates force on the rotor blades, which turn the shaft and allow the turbine to generate power.

section. The pressure at the exit of the combustor is at a much higher pressure than the exit of the turbine, and therefore the desired flow direction and natural flow direction are one and the same.

As stated before, all of these components work together towards a common goal: produce useful work. The difference between a good design and a bad one is simply how much fuel needs to be consumed to produce the required amount of work. To further understand this, the next section defines cycle efficiency and the role that each component plays in improving it.

## 4. Cycle Efficiency

In any thermodynamic system, the overlying goal is always to produce the maximum amount of work for a given amount consumed from an external energy source. The ratio between the amount of work produced and the amount of energy consumed is known as the efficiency of the system. For GT engines, it is more specifically known as the thermal efficiency, and it is defined as

$$\eta_{th} = \frac{W_{turb}}{Q_{comb}}, \tag{1.3}$$

$W_{turb}$ being the work produced in the turbine and $Q_{comb}$ the energy content of the fuel used in the combustor. GT engines have efficiencies typically around 30%; in other words, only about a third of the energy consumed through combustion is used towards generating power, and the rest is expelled out the back of the turbine. In order to harness this unused potential energy, particularly in power generation plants, the hot gasses exiting the GT engine are then used to help preheat the water used for a steam turbine. This combined cycle typically sees an overall efficiency boost up to around 50% [2].

To better understand thermodynamic systems, it is useful to model them with

idealized cycles. For GT engines, the Brayton cycle is used. Figure 6 shows a P-V diagram (pressure-volume) of the Brayton cycle.

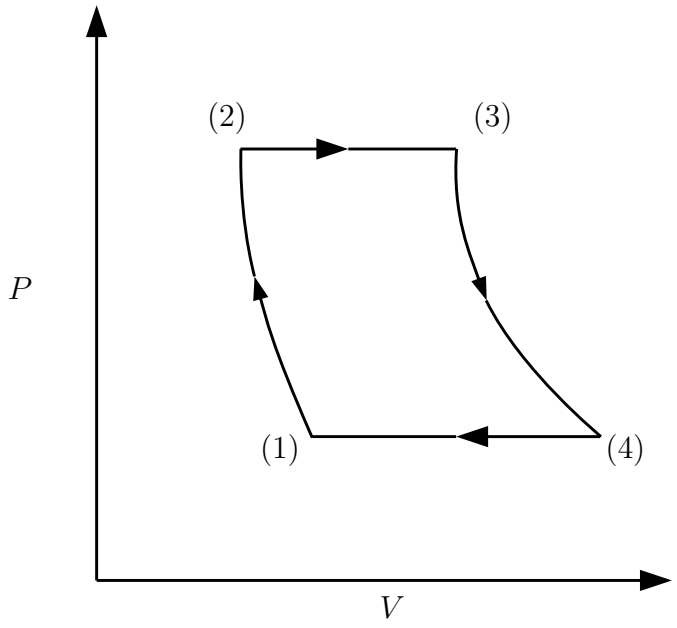


Fig. 6.: P-V diagram of the Brayton cycle. The isentropic compression (1-2), constant pressure heat addition (2-3) and isentropic expansion (3-4) are idealized processes for the compressor, combustor, and turbine, respectively. The constant pressure heat rejection (4-1) models the rejection of the hot gasses to the environment (which is replaced by cold air at the compressor inlet).

The Brayton cycle consists of the following processes:

- **Process 1-2:** Isentropic (i.e. no losses) compression
- **Process 2-3:** Constant pressure heat addition
- **Process 3-4:** Isentropic expansion
- **Process 4-1:** Constant pressure heat rejection

Upon inspection, the first three processes represent the compressor, combustor, and turbine, respectively. Process 4-1 models the rejection of the hot gasses to the environment to give a closed cycle. For any closed cycle, the net amount of work produced can be evaluated as

$$W_{net} = \oint P \mathrm{d}V, \tag{1.4}$$

where $V$ is the volume. Graphically, this expression is the same as the area under the curve of Figure 6. Thus, the Brayton cycle can be used to determine how each component contributes to the amount of work produced in the GT engine.

In the Brayton cycle increasing the differential between the low pressure point (states 1 and 4) and the high pressure point (states 2 and 3) allows more work to be produced. Thus, the compressor is a very important component of the GT engine. Also, increasing the volume, $V$, at the end of the combustion process (state 3) increases the amount of work production as well. The volume is directly proportional to temperature, and therefore, it is key to increase the temperature of the fuel-air mixture as much as possible during the combustion process. This is precisely why the design of the swirlers and dilution holes are so important, as they allow a more complete combustion to take place. Finally, an indicator for the performance of the turbine section is the exiting pressure of the fuel-air mixture. The compressor and combustor both have added large amounts of energy to the air, and now the turbine must recover all of that energy and convert it to useful work. This useful work is directly related to the pressure differential between the inlet flow to the turbine and the exit, and thus, the maximum amount of work that can be achieved is obtained from the lowering the pressure of the air back down to atmospheric conditions.

Of course, these are all idealized processes. Real GT engines experience deviations from this behavior, such as viscous losses in the compressor and turbine

and incomplete combustion in the combustion chamber. However, there are other real-world limits on the amount of work that a particular GT engine can produce. Those limits, and a more detailed look at the relationship between the combustor and turbine and how that relationship affects performance, are discussed in the next section.

## B. Limitations on Performance

The largest limiting factor for increasing GT engine performance is the melting temperature of metal used in the first stage turbine blades. In fact, the temperature of the gas exiting the combustor is already well above the melting temperature of the blade material, and referring to Figure 6, that temperature must be raised even higher to get higher power output. Advanced cooling techniques must be employed in order to minimize thermal stresses in the blade material. These cooling techniques typically use the cooler air from the compressor to form a film of protective air on the blade and on the wall that the blade is attached to. Taking this air from compressor lowers the total pressure of the air entering the combustor, thus lowering the thermal efficiency, and as the compressor pressure ratios increase, this "cooler" air will become hotter and hotter, thus making it less effective in cooling the turbine blades [3].

Another factor that makes the turbine blade cooling difficult is the highly turbulent nature of the flow exiting the combustor. Turbulent flows are chaotic in nature, and not only do they have increased heat transfer properties, they also have higher mixing properties [4]. This higher mixing tends to disrupt the film cooling of the turbine blades, effectively exposing the blades directly to the hot gasses from the combustor. Unfortunately, this highly turbulent behavior is directly a result of the high swirl that is imparted on the air entering the combustion chamber. As stated be-

fore, the swirling nature of the incoming air is responsible for creating a good mixture of the air and fuel, allowing complete combustion.

These competing factors make improving upon current GT engine designs a much more complicated task than simply studying the Brayton cycle. To improve the efficiency of these devices, designers need to be able to predict real engine exit characteristics of the flow exiting the combustor based on previously obtained data. The more detailed the data is, the better the models will be. The focus on the next section is the nature of the data that is needed, and the methods that are used to obtain it.

## C. Background on Numerical Techniques

The study of fluid flows and heat transfer is a complicated area. The general interactions that occur in real world fluid flows are still not understood very well, and so steps must be taken to at least be able to understand them for a system of interest. One method is experimentation. Experimentation would involve assembling the actual component to be studied (or at least a suitable model of it), and then measure the flow dynamics directly. A common example of this would be studying the flow over an airfoil in a wind tunnel. A scaled air foil is placed in a wind tunnel that accelerates ambient air to the desired velocity over the air foil. Then, measurements of pressure, temperature, and/or velocity can be made in a variety of methods (Goldstein [5] is a good source for the different types of measurement methods).

Experiments, when done correctly, are extremely useful, in the sense of "what you see is what you get." Once the instruments are calibrated and enough data is taken for statistical analysis, there is no need for the investigator to fret over whether the results are believable. However, a severe limitation of experimentation is that spatial

and temporal resolution is limited. Even with planar measurement techniques, it is extremely difficult to get highly resolved velocity, temperature, and pressure data for the entire flow field. Therefore, analysis is done before hand to determine the points of interest in the flow field, and this is where the focus is placed for measurement.

Conversely, a particular system may be investigated by numerical simulation. A set of equations, known as the Navier-Stokes equations, represent conservation laws in fluid flows. While analytical solutions to these equations are rare, they can still be solved numerically. This technique involves discretizing the domain into several smaller, more manageable sub domains and then solving the equations within each sub domain. With numerical simulation, the investigator can obtain three dimensional flow data that is also highly resolved in time. However, great care must be taken to ensure the flow information is realistic. Grid resolution, boundary conditions, and stability are all major concerns over whether the data obtained is accurate, and so typically numerical simulations must first be validated against experimental data, which somewhat defeats the purpose of the numerical simulation. Even so, numerical simulations are powerful tools, and studies that use both experimentation and numerical simulation can gather large amounts of data that is also trustworthy.

Computational fluid dynamics, or CFD, is the common name for numerical simulation of the Navier-Stokes equations. There are three main branches of CFD: Reynolds-Average Navier-Stokes (RANS), Large Eddy Simulation (LES), and Direct Numerical Simulation (DNS). The differences between the three are due mostly to how they handle turbulent behavior in the flow. In turbulent flows, the quantities of interest typically are the mean values of velocity, pressure and temperature and their fluctuating components (which are simply how the variable differs from its mean value with time).

In RANS, the velocity, temperature, and pressure terms are separated into their

mean and fluctuating components. Then, the entire equation is time averaged, and the resulting equation resembles the original, unaltered Navier-Stokes equations. However, an extra term is introduced that is termed the Reynolds stress, and unfortunately, this quantity is unknown. Therefore, to close the problem, the Reynolds stress is modeled, and the average quantities are solved for. Obtaining the correct model for Reynolds stress is difficult, and creates a good deal of uncertainty in the results. However, once the model is correct, this is simplest of the three methods to set up, and this method is the most widely used in industry.

On the other side of the spectrum, DNS resolves all scales, and the Navier-Stokes equations are solved directly with no modeling. Of the three, this is thought to be the most accurate, and with infinite computing resources available, the other two methods would not be necessary. However, because of the high resolution requirements of DNS, this method is impractical for most realistic flows.

In LES, the large turbulent structures are captured directly with no models, while the small structures are modeled. This approach is deemed more accurate than RANS since not all of the unsteady motions are represented through models, and the small scale motions are thought to be universal anyways, so they shouldn't depend on the geometry of the domain [4]. Whereas the resolution of DNS is so strongly dependent on the smallest scales of the flow, which decrease as the velocity speeds up, LES only needs enough resolution to capture the energy carrying structures, and thus has the advantage of a much lower computational cost. LES is a compromise between the two methods, allowing more realistic conditions to be simulated without the need for extensive modeling.

## D. Supercomputing

The complexity of any system can be defined by how many degrees of freedom (DOFs) it contains. A simple example of how one would define DOF would be with rigid body motion. If some object is hanging in space, with no constraints, then it has 6 DOFs. It can translate in three directions, as well as rotate in three directions. To understand how this object moves, one would need to be able to accurately describe its motion through these 6 components, which can be very difficult without any simplifications to the system. Alternatively, DOFs are also defined in CFD simulations. In CFD simulations, as mentioned before, the domain is discretized into smaller domains. Each sub domain can contain several gridpoints, which are where the Navier-Stokes equations are to be satisfied. Each unique gridpoint is a DOF. Therefore, the number of DOFs in a simulation can reach into the millions, and even billions, quite easily. Whatever numerical method is used, it must obtain solutions for all of these DOFs, and thus the computational cost quickly rises. While personal computers have become increasingly powerful over the past decade, they will only have enough power to compute the most basic of CFD problems.

Supercomputing is the solution to this problem. Supercomputers are vastly more powerful than typical consumer machines [6]. Some of the features that define supercomputers are

- Multiple computing cores (anywhere from 100s to 100,000s of cores)
- Large, high speed memory resources
- Efficient communication between computing cores

All three of these things play a role in how well a supercomputer performs, and therefore the magnitude of problem sizes it can handle. The biggest gains for super-

computing in the past few years have come from increased parallel efficiency. With parallel computing, problems are split over several computing cores, with each core handling only part of the problem. These cores run simultaneously, and if the cores are 100% efficient, then a solution for a particular problem will be obtained twice as fast if twice as many cores are used. This technology allows problems to be completed in a fraction of the time normally needed, allowing CFD to be a serious alternative in the design process, not just in academic research, but industry as well [7].

## E. Statement of Purpose

The study of energy and systems that generate power from energy sources continues to be an interesting yet challenging field. Gas turbines are just one example of machines that have been around for many years and yet still have much improvement that needs to be made. An important factor in the improvement of these machines is high quality, reliable data that designers can use to improve the various gas turbine components.

An area of study that has deficiencies in available data are combustors. The complex and volatile conditions inside the combustor make it difficult to take accurate measurements that span the entire geometry, and yet those same conditions also make numerical simulations in gas turbine combustors difficult. However, new advances in LES, as well the rise in supercomputing power, make combustor simulations viable.

The objective of this study is to validate the results of a Large Eddy Simulation in a model ring-type gas turbine combustor. With the model validated and method proven, spatially and temporally dense data sets can be taken and used to not only help improve the design of combustors, but also provide useful inlet conditions for use in turbine vane simulations.

# CHAPTER II

## LITERATURE REVIEW AND NUMERICAL METHODS

The goal of this study is the characterization of the complex flow regimes inside a model gas turbine combustor. A major focus for gas turbine researchers is the prediction of heat transfer and flow characteristics near the leading edge of the first stage turbine vane. The highly turbulent flow exiting from the combustor plays a significant role in those heat transfer characteristics, and yet there is a deficiency in the open literature on characterizations of the flow at the exit plane of the combustor. This is due, in part, to the large role that geometry plays in shaping the flow structures inside the combustor, making general conclusions on trends in the available data difficult. The lack of optical access in most combustor research models makes detailed measurements difficult. On the computational side, the wide range of length scales present in the flow make DNS too computationally expensive, but the unsteadiness of the flow, particularly near where the combustion takes place, makes RANS unsuitable as well.

This study combines the compromise between accuracy and computational cost that LES provides with the spectral accuracy and good convergence characteristics of spectral elements. The goal is the creation of a system that can give an accurate picture of the flow field in a relatively short amount of time. The present study will validate the model first with a simpler flow problem, but the once validated, future studies will extend it to more complex domains, both in terms of geometry as well as physics, which will give GT designers a more thorough data base to base their designs.

## A. Literature Review

In a gas turbine engine, the complex geometry and flow conditions inside the combustor create highly turbulent flow conditions at the exit plane. This flow, with a turbulence intensity that can reach 20 to 25% [3], has a large effect on the heat transfer characteristics near the leading edge of the first stage turbine vane. With increases in combustor technology, the temperature profile at the exit of the combustor now exceeds the melting temperature of the blade material in the first stage of the turbine, and so these vanes need to be actively cooled. In order to properly design these cooling systems, blade designers need an accurate description of the flow exiting the combustor.

Heitor and Whitelaw [8] obtained velocity, temperature, and concentration measurements in a can-type combustor, both for isothermal (non-reacting) and reacting cases. They concluded that the effects of combustion play a significant role in the behavior of the flow at the exit of the combustor. McGuirk and Palma [9] performed a parametric study on a water model of a can-type combustor. They provided detailed analysis on the vortex cores that form in the primary zone, and they concluded that these are direct result from both the swirlers as well as the dilutions jets. They also reported that the effect of swirl dampens out significantly as the flow moves downstream, and the flow approaches isotropic turbulence. Koutmos and McGuirk [10] performed a RANS study of an isothermal model of a can-type combustor, comparing the results to experimental data. They found good qualitative agreement in the flow structure, but noted that the model failed to predict the flow in areas of strong anistropic turbulence and large spatial variations.

Menzies [11] describes LES has having great potential for flows inside combustors, due to its explicit capturing of the large scale motions that transport momentum, as

well as its ability to resolve the unsteady jet-on-jet interactions. In addition, LES is suitable for capturing combustion effects because it already models sub grid scale (SGS) structures, which is typically where the chemical reaction are dominant. However, the main issue so far is that the computational cost of LES is much higher than that of RANS, thus making LES impractical as part of the design process. diMare et. al. [12] performed an LES on a can-type combustor found in the Rolls-Royce Tay engine. Qualitative velocity comparisons were made to previous experimental results, and combustion was modeled using scalar transport to investigate species concentrations. It was concluded that LES holds great potential in predicting flow patterns in real world conditions. Mahesh et. al. [13] successfully compared their LES algorithm to experimental results from a simple coaxial combustor as well as a complex gas turbine combustor that modelled one from a Pratt and Whitney engine. Kim et. al. [14] performed a blind feasibility study of a LES by comparing the prediction capabilities of a coarse grid simulation directly to experimental data, with the goal of obtaining results that were accurate enough to engineering standards. Results compared well to experimental data, matched much better than corresponding RANS results, and quality averaged data was able to be obtained overnight due to the coarsened nature of the grid. Jakirlic et. al. [15], like [10, 12], carried out a simulation on a combustor and compared it to experimental results. However, the combustor used by Jarkilic represents a more modern, ring-type design, and the code used for the simulation was a hybrid LES-RANS scheme, where RANS was used in near-wall region and LES was used elsewhere. The hybrid model was found to compare well to experimental results.

Staffelbach [16] notes that although LES simulations still carry a much larger computational cost than RANS, the rise of powerful parallel computing power has made LES a viable alternative to RANS. Whereas the previous studies employed finite element and/or finite volume approximations, the present study employs a spectral

element algorithm. NEK5000 [17] is a highly parallel, open source spectral element code developed to study turbulence. It has sustained high parallel performance up to 262,144 processors. The model used is a simplified segment of a ring-type combustor, yet contains all of the pertinent features such as high swirl characteristics and dilution jets. Velocity measurements in the primary zone, as well as qualitative flow visualizations, are compared to the experimental and numerical results obtained by Jarkirlic [15], as the two models are similar.

## B. Numerical Methods

The incompressible (constant density) Navier-Stokes equations in tensor notation, along with continuity, are

$$\begin{aligned} \frac{\partial u_i}{\partial t} + \frac{\partial \left(u_i u_j\right)}{\partial x_j} &= -\frac{1}{\rho}\frac{\partial P}{\partial x_i} + \nu \frac{\partial^2 u_i}{\partial x_j^2} \\ \frac{\partial u_j}{\partial x_j} &= 0, \end{aligned} \tag{2.1}$$

where $u_j$ represents the $j_{th}$ component of velocity and $\nu$ is the kinematic viscosity of the fluid being studied. The first, second, and third components, $j$, correspond to the $x$, $y$, and $z$ Cartesian coordinates, respectively. A useful parameter that can be used to quantify the complexity of a given flow is the Reynolds number, $Re$. The Reynolds number is a non-dimensional number defined by $Re = \dfrac{U_\infty L}{\nu}$, where $U_\infty$ is the characteristic velocity and $L$ is the characteristic length. It is often up to the investigator to decide what to choose for $L$, but some common examples are the diameter in a pipe flow, the height in a channel flow, or the blade chord (distance from one tip to the other) for flow around a turbine vane. In CFD, the Reynolds number can be used to predict the grid resolution required to capture all of the length scales. As identified by Kolmogorov, the ratio between the smallest length scale and largest

is on the order of $Re^{-3/4}$. Thus, as the Reynolds number increases, the grid spacing must decrease to ensure that all of the relevant scales are captured and ultimately increasing the number of grid points needed [18].

This requirement is what prevents DNS simulation of most realistic flow conditions, like those encountered in GT engines. These scales must be captured in some manner in order for a simulation to give realistic results. Small scale fluctuations are responsible for energy dissipation: without these phenomenon accounted for in a simulation, the energy that is transferred from the larger scales to smaller scales will tend to build up. At the very least, this will cause the flow to exhibit nonphysical characteristics, but it could cause the simulation to be unstable and crash.

Berselli [18] suggests that instead of spending large computational resources to capture these small eddies and obtain the true solution to the Navier-Stokes equations, one can instead seek an approximate solution that represents a spatial average of the true solution. This allows for the domain to be much coarser, saving on computational costs. The standard setup of a LES model, as well as the specific model for the present study, are detailed in the following.

With the LES model, a spatial filter is applied to the Navier-Stokes equations to obtain

$$\begin{aligned} \frac{\partial \bar{u}_j}{\partial x_j} &= 0 \\ \frac{\partial \bar{u}_i}{\partial t} + \frac{\partial \left(\bar{u}_i \bar{u}_j\right)}{\partial x_j} &= -\frac{1}{\rho}\frac{\partial \bar{P}}{\partial x_i} + \nu \frac{\partial^2 \bar{u}_i}{\partial x_j^2} + \frac{1}{\rho}\frac{\partial \tau_{ij}}{\partial x_j}, \end{aligned} \tag{2.2}$$

where the overbar denotes spatial filtering, and $\tau_{ij} = \rho\left(\overline{u_i u_j} - \bar{u}_i \bar{u}_j\right)$ is the subgrid-scale (SGS) stress tensor. This term can not be calculated with the resolved scales, and so it must be modeled [13]. One of the more popular choices for the SGS stress

tensor is the eddy viscosity model,

$$\frac{1}{\rho}\frac{\partial \tau_{ij}}{\partial x_j} \approx \frac{\partial}{\partial x_j}\left(\nu_t \bar{S}_{ij}\right), \tag{2.3}$$

where $\nu_t$ is the eddy viscosity and $\bar{S}_{ij} = \frac{1}{2}\left(\frac{\partial \bar{u}_i}{\partial x_j} + \frac{\partial \bar{u}_j}{\partial x_i}\right)$ is the strain rate tensor on the filtered velocity. This is not unlike how RANS simulations solve the closure problem. One of the first eddy viscosity models for LES (and still most common) is the Smagorinsky model, which defines the eddy viscosity as

$$\nu_t = \left(C_s \Delta\right)^2 \left|\bar{S}_{ij}\right|, \tag{2.4}$$

where $C_s$ is the Smagorinksy coefficient and $\Delta$ is the filter width. While this model held great promise, it has been found that the value used for $C_s$ (0.17) is too large, and thus the eddy viscosity term dissipates too much energy. This strong dissipation can essentially wipe out larger scales, drastically changing the makeup of the flow field.

In order to contain the large amounts of dissipation present in the Smagorinsky model, modifications have been made that allow $\nu_t$ to adapt to flow conditions with the hopes of better matching to DNS and experiments. Examples include allowing $C_s$ to tend to 0 near walls or allowing $C_s$ to change with spatial location and time. The present study employs a high pass filter (HPF), such that [19]

$$\begin{aligned} \tilde{u}_j &= H * \bar{u}_j, \\ \nu_t^{HPF} &= 2\left(C_s \Delta\right)^2 \left|\tilde{S}_{ij}\right|. \end{aligned} \tag{2.5}$$

Here, the terms with a tilde are the high pass filter versions of the spatial average terms, $H$ is the high pass filter function, and $\left|\tilde{S}_{ij}\right| = \sqrt{2\tilde{S}_{ij}\tilde{S}_{ij}}$. The driving force behind the use of LES is the idea that at small scales, the eddy patterns behave in one

geometry as they would in a different one; that is, they are self similar. Therefore, it makes sense to use only the smallest resolved scales to model the unresolved scales, as this interaction is what really needs to be modeled. Figure 7 demonstrates visually the method being used. The HPF Smagorinksy model satisfies two important criterion.

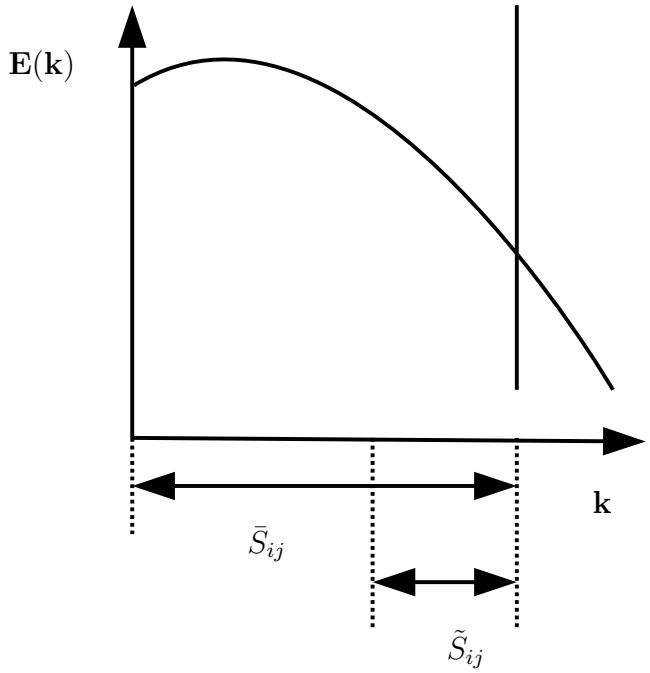


Fig. 7.: Visual description of HPF Smagorinsky model. The abcissa, $\mathbf{k}$, is the frequency, and the ordinate, $\mathbf{E}(\mathbf{k})$, is the energy contained in a particular frequency. In an LES model, the highest frequency components (depicted to the right of the vertical line) are not captured by the grid points, while everything to the left is captured. In a standard Smagorinsky model, the term $\bar{S}_{ij}$ is used to calculate the eddy viscosity, while the HPF Smagorinsky model uses only the highest frequencies captured by the grid, $\tilde{S}_{ij}$.

First, the eddy viscosity vanishes in laminar regimes, allowing it to be more useful in transitional flows than the standard Smagorinky model and even the dynamic

Smagorinsky model. The other criteria satisfied is that the eddy viscosity is predicted to disappear near walls because $\tilde{S}_{ij}$ vanishes [20]. This alleviates any need for the near wall damping functions mentioned before.

Now that the Navier-Stokes equations have been filtered, the next step is solve for the spatially averaged velocity and pressures. The technique used for solving the filtered Navier-Stokes equations is typically the point of departure from one algorithm to the next. The discussion of those algorithms, and the one used for this study, is now presented.

## C. Numerical Solution of Navier-Stokes

While there are numerous approximation techniques, this section will focus on only two that are very similar to each other: the finite element method (FEM) and spectral element method (SEM). The basic premise for each technique is to split the domain into smaller sub domains, or elements, and then approximate the solution in each element while ensuring that interelement continuity is maintained (i.e., the solution "matches" at element boundaries). In order to make the calculations robust, each physical element is typically transformed to a master element. In one dimension, this master element is a line segment that spans from -1 to 1, and higher dimensions are just extensions of this principle. For clarity, the technique will be shown for one dimension, where the master element coordinate is $\xi$. Within each master element, the solution is approximated as

$$u^e \approx u_N^e(\xi) = \sum_{n=0}^{N} a_n \phi_n(\xi). \tag{2.6}$$

Here, $u^e$ is the solution in a particular element (not to be confused with $u_j$, the velocities in the Navier-Stokes equations), $\phi_n$ are interpolation polynomials, $a_n$ are

the coefficients that need to be solved for, and $N$ is the polynomial order to be used within the element. These interpolating polynomials are constructed as

$$\phi_n(\xi) = \prod_{i \neq n} \frac{\xi - \xi_i}{\xi_n - \xi_i}. \tag{2.7}$$

$\xi_n$ are the set of points on the master element where the function is interpolated (i.e., the locations that correspond to $a_n$). This formulation produces $\phi_n$ such that

$$\phi_n\left(\xi_j\right) = \begin{cases} 1 & : j = n \\ 0 & : j \neq n \end{cases} \tag{2.8}$$

In other words, each polynomial is zero at all interpolation points except its own. This is important, because now the coefficients $a_n$ directly correspond to $u_N^e\left(\xi_n\right)$.

For FEM, the approximate functions are interpolated on a uniform grid with a spacing of $\frac{L_e}{N}$, where $L_e$ is the length of the element. Figure 8 shows two examples of finite elements, one of polynomial order one and the other at two, with their respective interpolating functions. Usually, FEM algorithms employ 2nd order elements at most,

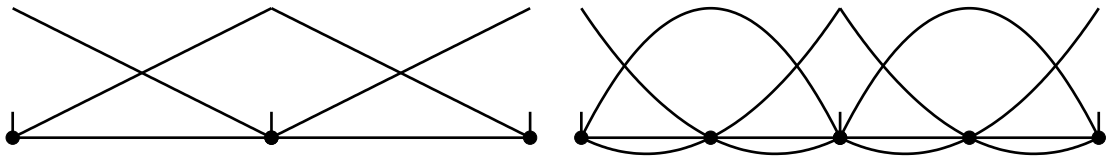

Fig. 8.: Example of finite elements. Two elements of polynomial order 1 are shown on the left, and the right shows polynomial order 2

and if the solution accuracy is not acceptable, then the element size is reduced. Higher orders, approaching six and beyond, begin to become problematic because of the use of uniform interpolation points. The polynomials begin to overshoot near the endpoints (meaning becoming much larger than one), causing the interpolation to incur error

at an unacceptable level.

Spectral elements differ mainly in what is used for the interpolation points. For calculations using the spectral *method*, the solution for the whole domain is approximated by an orthogonal basis, such as Chebyshev ($T_n$) or Legendre ($L_n$) polynomials. For most bases used for SEM, the interpolation points are not uniform. For example, for Legendre polynomial, the points used are the solutions to

$$\left(1-\xi^2\right) L'_N\left(\xi\right) = 0, \tag{2.9}$$

where $L'_N$ is the derivative of the highest order Legendre polynomial used in the element. These points are known as the Gauss-Lobatto-Legendre (GLL) points. In other words, the interpolation points used are the endpoints as well as the zeros of $L'_N$. This results in the interpolation points being pushed towards the endpoints, which curbs the overshoot seen in uniformly spaced points. Figure 9 demonstrates this for a polynomial order of 6. One advantage from using spectral element is the

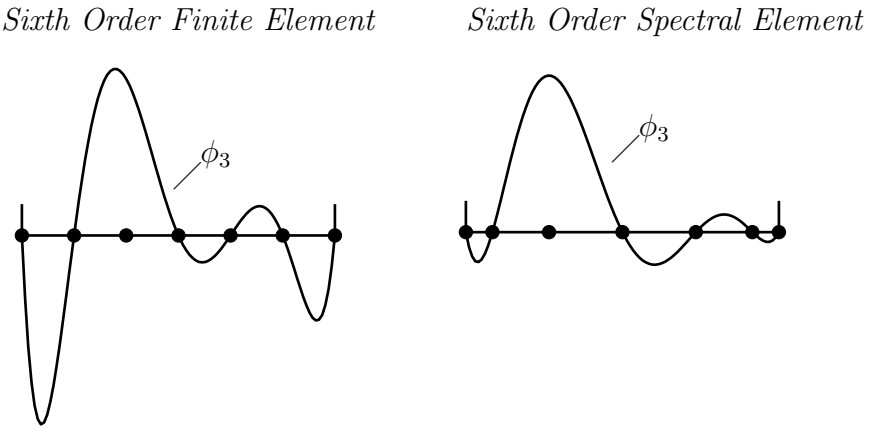


Fig. 9.: Comparison between finite and spectral elements. Only $\phi_3$ is shown for clarity. Even at a modest polynomial order of 6, the finite element (left) features significant overshoot near the boundaries.

rate of convergence. The convergence rate for FEM is typically 2nd order. However, for SEM, the convergence rate starts at 2nd order, but quickly increases to 7th or 8th order as the polynomial order used gets higher. This means that for a certain accuracy requirement, SEM will require far fewer grid points than FEM. In the context of supercomputing, this is a great benefit, as more complicated problems can be handled in a shorter amount of computing time relatively. Also, because there are fewer elements, the amount of inter-element communication decreases as well, increasing speed overall on parallel machines. Deville [21] may be referenced for more information on spectral elements.

The ability to gain an understanding of the flow physics in a particular domain efficiently and accurately is what makes spectral element algorithms interesting. Already, the advantages inherent to spectral elements have caught the attention of developers who want to create massively parallel codes. One such code is NEK5000 [17], which has begun to gain traction in academic research. Built from the beginning to take advantage of the speed increases afforded to spectral element calculations, NEK5000 has been used by many researchers to study a wide range of problems. The speed and accuracy of NEK5000 makes it an ideal choice for this study. NEK5000 has recently been compared to an open source finite volume code, OpenFOAM [22], using a standard benchmark, turbulent flow in a channel. The study found that NEK5000 had greater scaling (i.e., scaled efficiently out to a larger number of cores). However, more importantly, it was found that for a given accuracy level, OpenFOAM required more than double the grid points in the wall normal direction [23]. This demonstrated the true power of a spectral element solver such as NEK5000.

## D. NEK5000

NEK5000 is a highly parallel, open source spectral element code for solution of the Navier-Stokes equations. It uses high order, yet flexible elements to be both robust and to cut down on element-to-element communication. It also uses matrix conditioning and solution techniques such as conjugate gradient to further increase its speed. While NEK5000 is set up for DNS solutions by default, modifying it to become an LES solver is not too arduous of a task.

Along with the source code, a typical problem set up for NEK5000 is maintained by four main files: the *rea* file, the *SIZE* file, and the *usr* file,. The *rea* file provides the problem parameters, such as fluid properties, time step size and number of steps to run, and the mesh information. The *size* file contains information that gives information on how many processors to run on and the polynomial order of the basis functions used in the simulation. The focus of this discussion will be on the *usr* file, as this is where the LES model is implemented.

The *usr* file contains several base functions that are called by NEK5000 during a simulation. Some functions are called only once, while others are called every time step. They are included in a separate file, instead of inside the main source code, so that the user can make use of them. For instance, the *userbc()* function allows the user to provide functions and decision-making structures to describe the boundary conditions of their domain. The function *userchk()* is called every time step. Here, the user can do anything from calculate averages and other quantities of interest that are derived from the flow field to even modifying the flow field, such as adding acceleration at the outflow boundary. The *usr* file also allows for users to supply their own functions that are then called by the base functions. This way, the file becomes more manageable, as commonly used pieces of code can be stored in user defined

functions instead of being placed directly in the base functions.

The *usr* file is the base where the LES model is implemented in the present study. Figure 10 provides a diagram of the implementation of the HPF Smagorinsky LES model. The base function *userchk* calls the user defined function *eddy_visc* for each

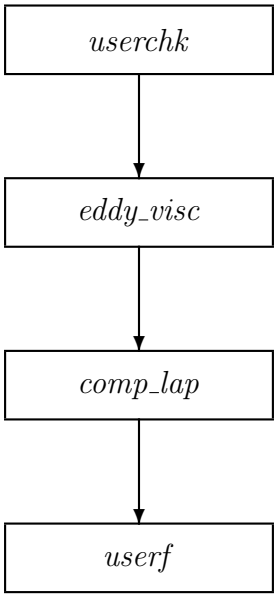


Fig. 10.: Diagram of LES implementation in NEK5000. *userchk* first calls *eddy_visc* on an element by element basis. This function calculates $\nu_t^{HPF}$ using the steps given in Equation 2.5. *userchk* then calls *comp_lap* on an element by element basis, calculating $\tilde{S}_{ij}$. Finally, when *userf* is called by the main program, where the newly calculated $\tau_{ij}$ is implemented as a forcing function for each element calculation.

element in the domain. Inside *eddy_visc*, the HPF function is set up and then the velocity is filtered. The filtered velocity is then used to calculate the filtered strain rate tensor, and along with the filter width (calculated from a built-in NEK5000 function) and a constant $C_s$ of 0.1, the eddy viscosity is calculated. Next, the filtered strain rate tensor is again calculated using the *comp_lap* routine. Finally, the filtered

Table I.: Dimensions of the combustor domain

| | |
|---|---|
| Width | $W = 0.83$ |
| Height | $H = 1.00$ |
| Length | $L = 3.00$ |
| Nozzle Diameter | $D = 0.25$ |
| Dilution Diameter | $d = 0.10$ |

strain rate tensor and eddy viscosity are multiplied with each other and inserted into the right hand side of the Navier-Stokes equations via *userf* as a forcing function.

## E. Geometry

Figure 11 shows the combustor domain with the boundary conditions highlighted. The domain shown represents a slice of a ring-type annular combustor: several of these domains connected together in the periodic direction would form a full combustor ring. The domain features velocity inlets for both the flow exiting the swirl nozzle and for the secondary flow that enters through the dilutions holes, and the domain is periodic in $y$. An artificial exit section is added at the exit of the combustor. Non-trivial divergence is added to the outlet to ensure that there is no back flow, as this can cause the simulation to be unstable. The remaining boundary faces in the domain are set as no-slip walls.

The dimensions of the domain are given in Table I. All dimensions given are normalized by the channel height, $H$. The swirler velocity is prescribed in polar

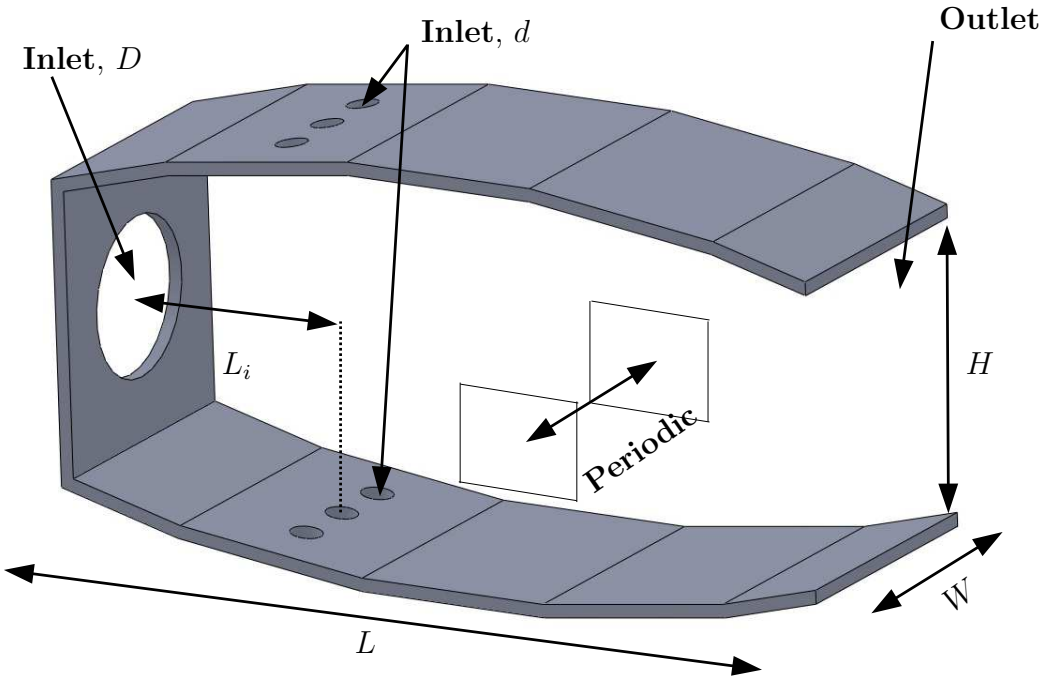


Fig. 11.: Computational domain of combustor. The boundary conditions are in bold face, and important dimensions are shown. A example pair of matching periodic elements is shown, although their size is greatly exaggerated. The origin of the domain is at the center of the swirler, with $x$ as the axial direction, $y$ in the periodic direction, and $z$ in the wall normal direction

coordinates as

$$\begin{aligned} u_x &= 6.75 u_{x,max} \left(r^2 - r^3\right), \\ u_r &= 6.75 u_{r,max} \left(r^2 - r^3\right), \\ u_\theta &= 0.85, \frac{2r}{D} > 2/3. \end{aligned} \tag{2.10}$$

Here, $u_x$, $u_r$, and $u_\theta$ are the axial, radial, and circumferential components of velocity, $u_{x,max} = 1.044$, and $u_{r,max} = 0.603$. The circumferential component is responsible for the amount of swirl that the swirler geometry imparts on the incoming air, and so it is an important parameter to model. The swirl number, $S$, is defined as the ratio between the circumferential momentum flux to axial momentum flux, and for this study, it was approximately unity. The effect that the dilution jets have on the overall flow is quantified by another dimensionless parameter, $J$, which is the momentum flux ratio between the dilution jets and the bulk flow in the channel. Finally, this study matches to the Reynolds number given in [15] as 11,000 based off the bulk velocity in the combustor ($U_\infty$). All three of these numbers are matched based on the inlet boundary conditions and the geometry of the domain, so there is no need for complicated controls in the *usr* file.

## F. Mesh Generation

With any CFD simulation, the meshing process is one of the most important tasks to get correct. The most robust, efficient algorithms are still heavily dependent on having good mesh quality, and NEK5000 is no exception. NEK5000, at this point, has two main requirements for the mesh:

- The elements must either be fully quadrilateral (2D) or fully hexahedral (3D)
- The elements must form a conformal grid

Hexahedral (hex) elements are a good choice in the sense that they are geometrically flexible. On boundaries that have large curvatures, it takes far fewer hex elements to conform to the boundary than it does tetrahedral (tet) element, in general. Figure 12 illustrates what is meant by conformal grid with a simple 2D example. This requirement makes the calculation at the boundaries simple, since the interpolation function on the boundary of the left element is exactly the same as the one for the right element (they will have the same GLL points). With a hanging node, however, the solution at that point must be interpolated from the other two. If there are many hanging nodes in the domain, this can increase the overhead for the element calculations. However,

(a) Example conformal grid (b) Example non-conformal grid

Fig. 12.: Example of conformal and non-conformal grid. The non-conformal grid has a "hanging node" in the middle of its neighboring element, which needs to be interpolated for each step.

although conformal all-hex grids are nice for computations, they take much more work to build, and there are no automatic solutions available. The geometry must be separated into several smaller volumes that are easily meshed. Also, since the mesh is conformal, it is more difficult to do adaptive refinement, which is a localized re-

finement in areas that need more resolution. Typically, this finer resolution will need to propagate out along what are known as chords, as shown in Figure 13. The final

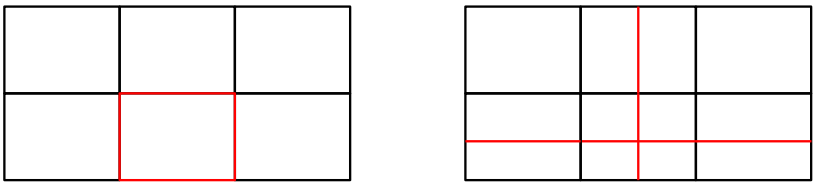

Fig. 13.: Example of adaptive mesh refinement. If the element highlighted in red on the left needs more resolution, then that refinement will need to propagate along chords in NEK5000, due to its lack of support for non-conformal grids.

complexity in using an all-hex mesh for this domain is due to the circular faces. Both the nozzle and the dilution jets are modeled as circular faces. Constructing a mesh on a quadrilateral surface is done simply by connecting points on the boundary that are opposites. However, this will not work for circles. Higher complexity face meshing algorithms could be used, such as PAVE, and then the resulting mesh could simply be extruded (using the Cooper tool) in the direction normal to the inlet. However, this method will not work for this geometry. The normals of the swirler inlet and the dilution holes are orthogonal to each other, and thus the Cooper tool cannot be used (the extrusions from the swirler inlet and the dilution inlets effectively coolide, and the Cooper algorithm is not robust enough to handle this). Instead, the circle is split into a square in the middle of the circle and then four other pieces formed by connecting the corner points of the square diagonally to the circle. Figure 14 demonstrates this structure.

There were two meshes used for this study, one for $J = 0$ and one for $J = 100$. While the same mesh could have been used for both cases, the dilution holes were

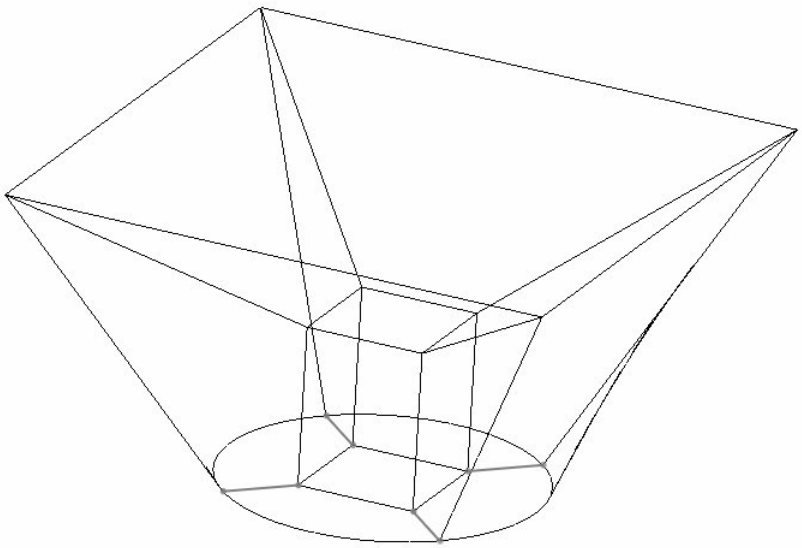

Fig. 14.: Example sketch of coarsening structure for circular faces. The circular face is first split into 5 segments. The central segment is extruded out, and then that face is expanded outwards. The other four faces of the mesh form volumes with the eight faces that are created from the first extrusion.

Table II.: Element counts and polynomial order for each case

| Case | $J = 0$ | $J = 100$ |
|---|---|---|
| Element Count | 18,897 | 23,530 |
| Polynomial Order | 7 | 7 |

removed for the first case, resulting in a significant savings on element count (and complexity). The element count and polynomial order are given in Table II. Figure 15 shows a three dimensional view of the mesh for the $J = 0$ case (i.e., with no dilution jets). An important lesson learned in this study is the effect of mesh quality on LES simulations. Although mesh quality is important in all CFD simulations, LES simulations can easily suffer from a poor quality mesh, such as large aspect ratios or highly skewed elements. This is due to how $\nu_t$ is calculated. If a mesh cell is bad, then not only are the average terms affected, but the HPF terms as well. These two items combined can cause simulation blow ups, even for cases with relatively simple flow physics such as this first case. Figure 16 shows two planar slices of the mesh to demonstrate the coarsening structure used for the swirler inlet. Roughly speaking, this structure results in a reduction in element count by more than 50%, so even though it wasn't necessary for this case, the benefits from this structure are quite clear.

For case 2 ($J = 100$), the dilution jets are added, and so more coarsening structures had to be placed on the dilution inlets. Figure 17 shows a three dimensional view, where the jet inlets can be seen at the top of the combustor domain. Figure 18 provides a visual explanation for why the coarsening structures are not only helpful

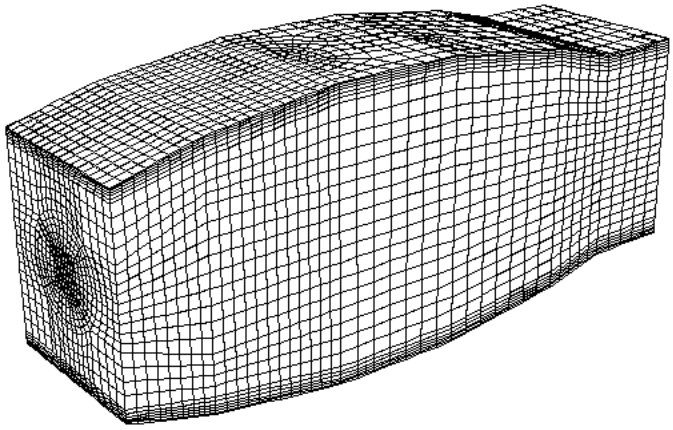

Fig. 15.: Mesh of domain for first case, $J = 0$. The total element count is 18,897 and polynomial order is 7, giving 6.4 mo. degrees of freedom.

in terms of total element count, but are also necessary for this problem. From the figure, a savings in element count is provided from coarsening structures on the dilution jets. It is difficult to calculate the element savings from using coarseners at both the swirler inlet and dilution inlets compared to no coarseners at all, since this type of mesh would not be allowed (or is at least difficult to comprehend). However, roughly speaking there is a savings of approximately 30% from using the coarseners at the dilution jets.

With the domain meshed and the boundary conditions properly set, the simulations can now be run to gain results. The following chapter gives those results, along with the direction this study is headed in the future.

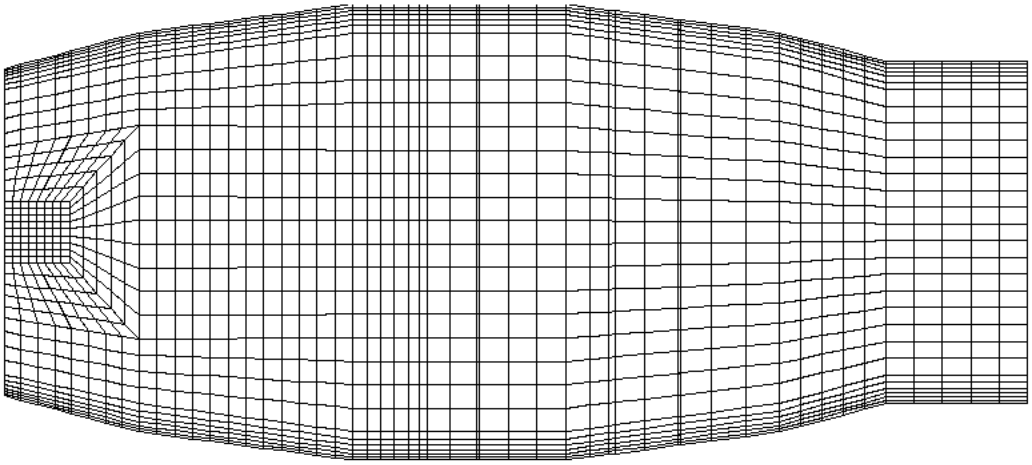

(a) Slice at $y = 0$

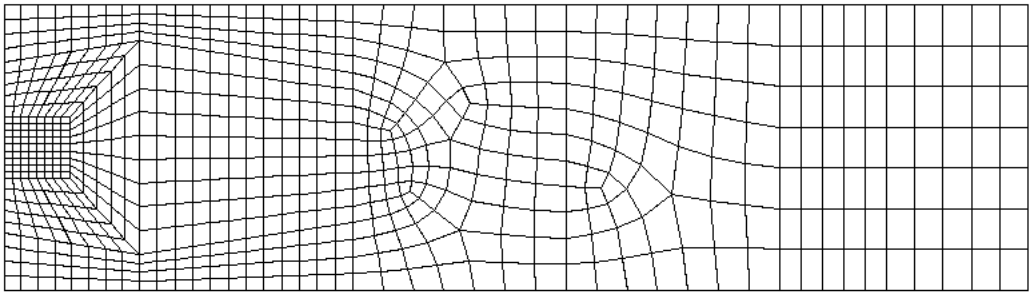

(b) Slice at $z = 0$

Fig. 16.: Slices of mesh for $J = 0$ case. The effect of the coarsening structure can be seen in the slices. The coarsening structure, while not necessary in this first case, roughly reduces the number of element needed by half.

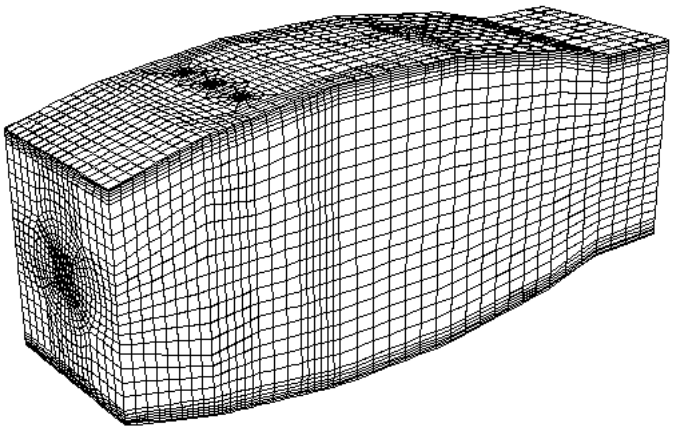

Fig. 17.: Mesh of domain for second case, $J = 100$. The total element count is 23,530 and polynomial order is 7, giving 8.0 mo. degrees of freedom.

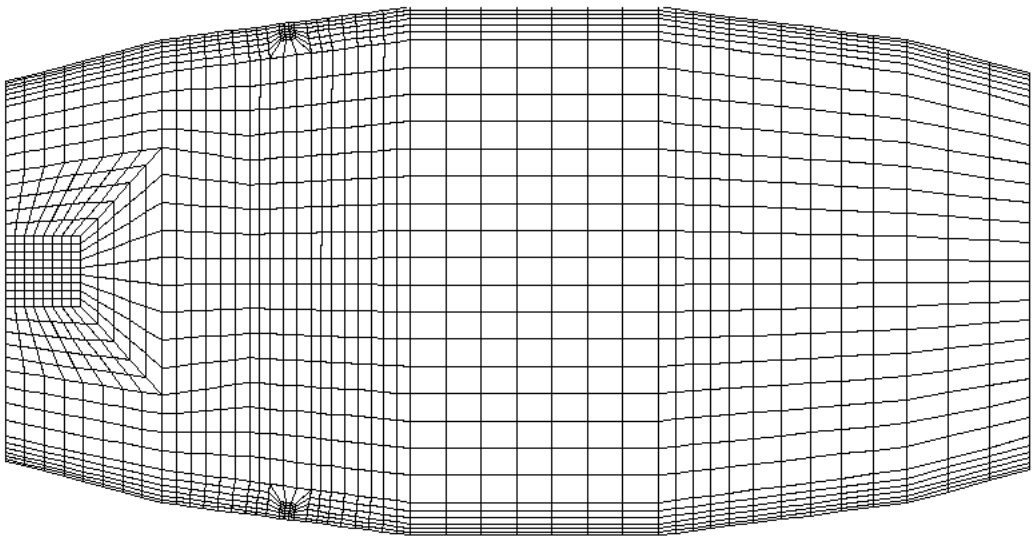

(a) Slice at $y = 0$

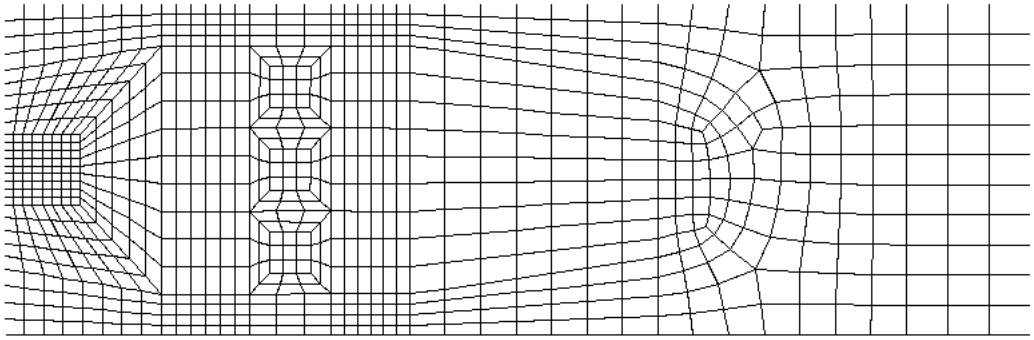

(b) Slice at $z = 0$

Fig. 18.: Slices of mesh for $J = 100$ case. For this case, the coarsening structure for all inlets is necessary because Cooper extrusions from the inlet faces would intersect.

# CHAPTER III

# RESULTS AND DISCUSSION

The following gives the progress on the current study, for the case with $J = 0$ (no dilution holes) and the case with $J = 100$. Both of these cases are compared to Jakirlic [15]. The flow geometries are slightly different, with Jakirlic's chamber being a simple channel but employing a full swirl nozzle, but several qualitative and some quantitative comparisons are made.

Presently, both cases have a total combined run time of approximately 40,000 hours. Both cases were run on 256 processors at Texas A&M's supercomputer EOS.

## A. Convergence Study

In order to trust the results obtained from a simulation, the convergence of the algorithm must be checked. The common way of saying this is ensuring the algorithm agrees with itself; that is, the solution doesn't change if the resolution is increased. Because the types of problems and flow situations studied in CFD analysis rarely have direct, analytical solutions to the Navier-Stokes equations, the error in a simulation can only be estimated by assuming a relatively high order run is the "true" solution. Then, it is simply a matter of running the simulation multiple times at different resolutions to determine whether the error is reasonable enough, and more importantly, that no important flow features are being missed due to under resolution.

The convergence study performed for the $J = 0$ case is shown in Figure 19. The error is slightly higher than what would be preferred, but the exponential convergence can still be seen in the figure.

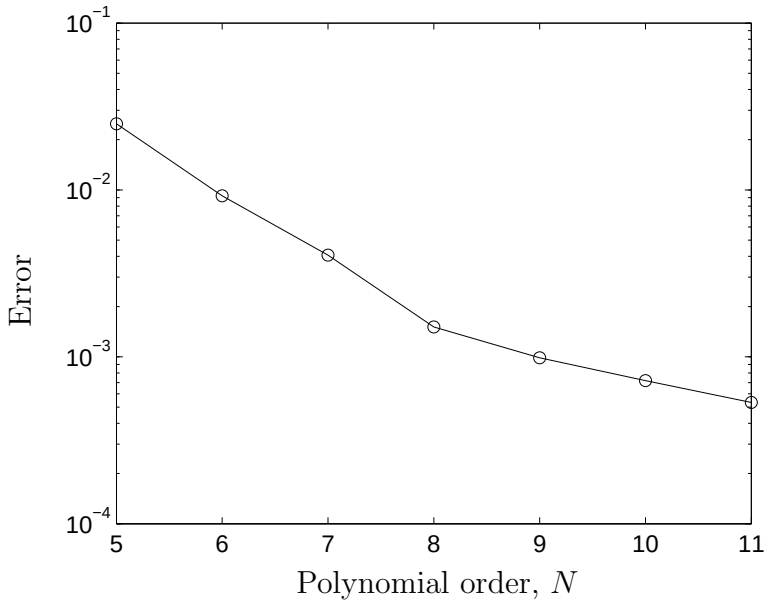


Fig. 19.: Convergence study for $J = 0$ case. Exponential convergence is shown from the nearly constant slope on the semilog plot. Results were taken from polynomial order 7, and the true solution was assumed to occur at order 13.

## B. Results for $J = 0$ Case

Figure 20 shows the axial velocity profile in the horizontal midplane at several locations near the swirler entrance. Also shown is experimental data reported by Jakirlic. Jakirlic also featured a hybrid LES-RANS solver. The solver agreed quite well with their experiment, and so that data is not included here for the sake of clarity.

In NEK5000 case studies, typically the flow parameters are normalized. Hence, the maximum inlet velocities are approximately unity, as well as the dimensions. The study done by Jakirlic used boundary conditions that were a direct result of what was seen in the experiment. Thus, the velocity magnitudes of this study and theirs will not match, but the overall behavior should. The data shown in Figure 20 is normalized by the bulk velocity, $U_b$, which is the average velocity over the cross section of the channel (in the $y$-$z$ plane). This factor is also used in the other plots. The present study and the work of Jakirlic exhibit similar characteristics: the axial velocity has strong peaks near the entrance which levels out further down the combustion chamber. This is indicative of the Precessing Vortex Core (PVC), a large vortex structure that stems from the high vorticity created in the swirlers. This structure is important for flame stabilization as well as to promote better mixing. However, the distribution in the present study appears to spread towards the periodic walls much more rapidly than Jakirlic's. This can be explained by differences in the geometrical setup. Both the experimental rig and the subsequent CFD simulation were done on a channel with a square cross section, i.e. the height ($H$) to width ($W$) ratio was unity. The present study employed a domain that models actual gas turbines more closely, although it is still simplified greatly. The physical dimensions of the current domain are normalized by the height at the exit of the combustor, giving a width of 0.833 and a height that ranges from 1 to 1.6. Therefore, a possible reason for the discrepancy in Figure 20

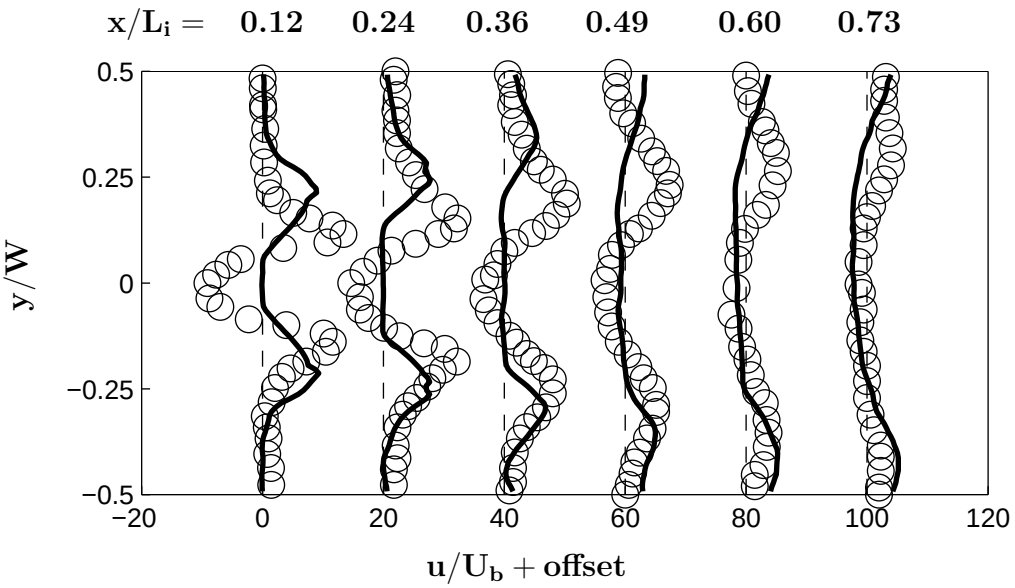


Fig. 20.: Axial velocity distributions in the horizontal midplane for $J = 0$ case. The axial ($x$) distance is normalized by the entrance length, ($L_i$), and the planar ($y$) distance is normalized by the width of the domain, $W$ The present study's results are shown by the solid line, while the normalized experimental results from Jakirlic [15] are shown with circles. Although the structures are similar in appearance, the distribution in the current study appears to dissipate towards the periodic boundaries much more quickly

is that the width of the current domain is not wide enough to capture the entire distribution. If the $y$ coordinates of the present study are normalized to emulate a domain with a unity height to width ratio at the location where the jets will be, the results appear to be much better, as seen in Figure 21.

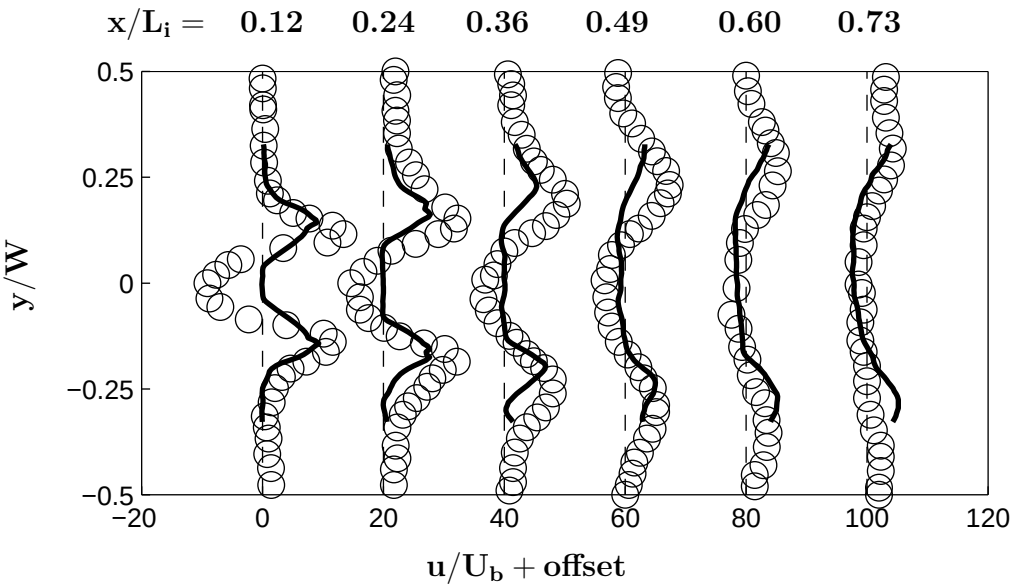


Fig. 21.: Axial velocity distributions in the horizontal midplane for $J = 0$ case, with geometrical adjustments made. The adjustment made to the current results show that this study's domain was not created wide enough to capture the full velocity distribution. However, the portion it did capture follows the data reported by Jakirlic [15] fairly well.

Figures 22 and 23 show time-averaged streamlines set over a contour of axial

velocity. The strong back flow region is readily seen here. An interesting feature is the lack of symmetry in the backflow region. This may be due to the domain not being wide enough, but Jakirlic does show evidence in their experiment that the segments of a ring-type combustor are not fully periodic, and this may be an example of that.

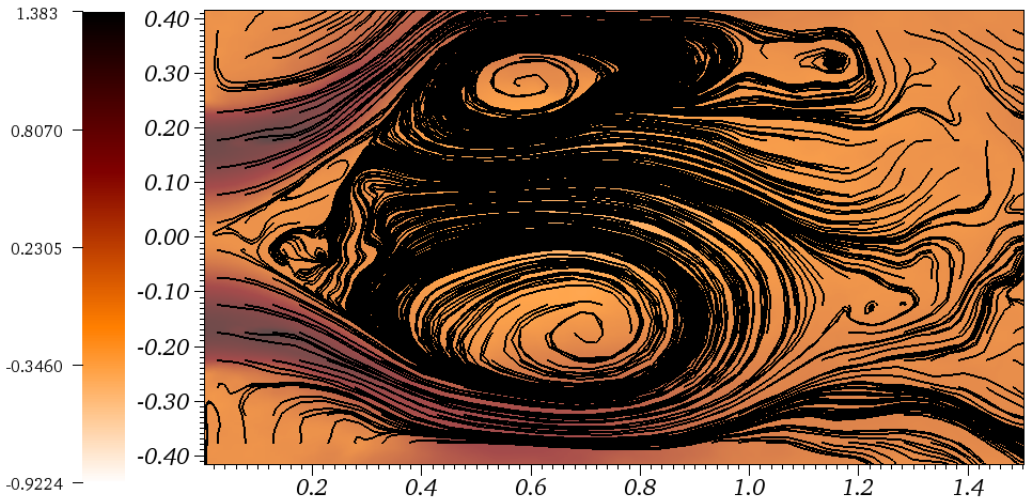


Fig. 22.: Time averaged streamlines and axial velocity contour in horizontal mid-plane for $J = 0$. The data is time-averaged over 8.4 seconds. The figure shows the recirculation zone caused by the Precessing Vortex Core. The plot also hints at the possibility that the combustor is not purely periodic, the backflow region in the flame stabilization zone may oscillate. Only the first half $(L/2)$ of the domain in the axial direction is shown for clarity.

Figure 24 shows profiles of streamwise stress component for both the present study and the experiment by Jakirlic. The data is sampled in the $y$ direction at the same axial locations as Figure 21. Like before, the current study's data is scaled to account for the domain being too narrow to assume periodic conditions, and the stress

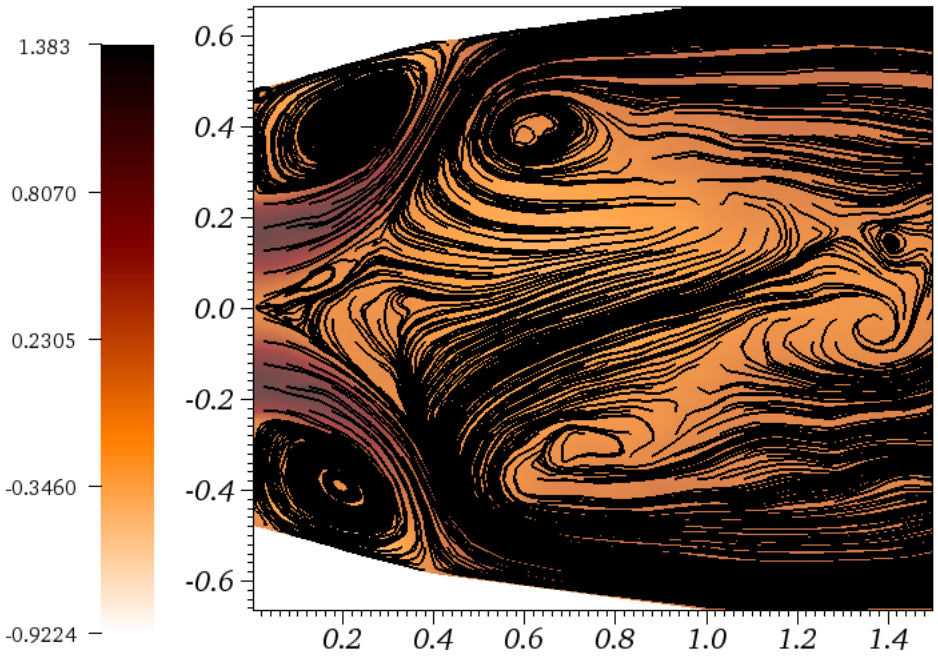


Fig. 23.: Time averaged streamlines and axial velocity contour in vertical midplane for $J = 0$. The data is time-averaged over 8.4 seconds. The lack of dilution jets cause the velocity to be slammed into the combustor wall, which could cause problem in terms of thermal wear for the combustor lining. Only the first half $(L/2)$ of the domain in the axial direction is shown for clarity

components from Jakirlic and from the present study are also normalized by their respective bulk velocity. Likewise, Figure 25 is a plot of the shear stress component

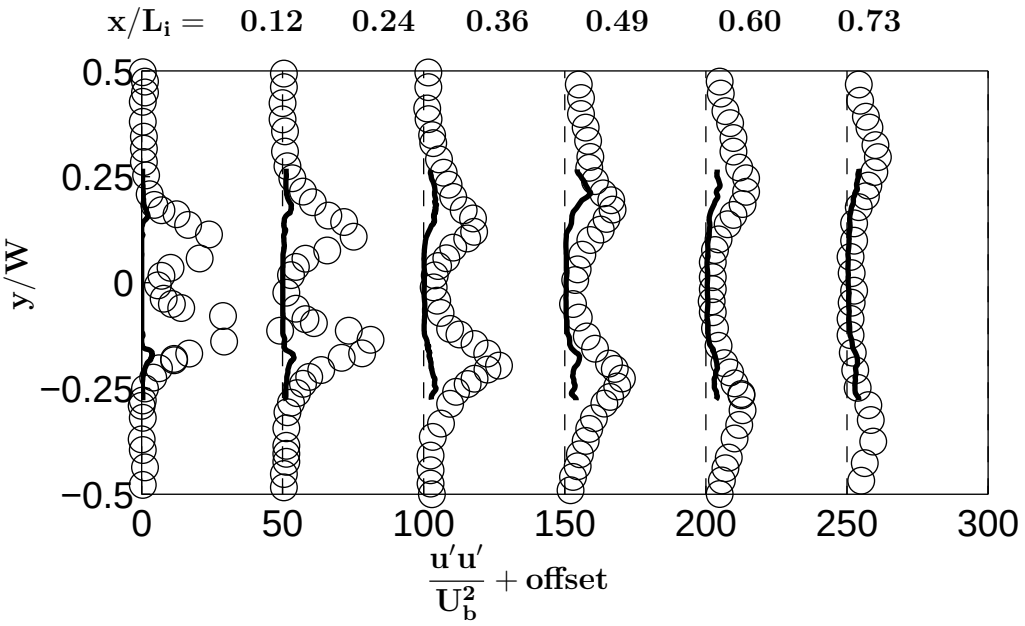


Fig. 24.: Plot of streamwise stress component profiles and comparison to previous data. There is poor agreement between the present study and Jakirlic [15] in terms of the magnitude the stress component, showing that the velocity boundary condition given for this study is does not emulate the swirler component given in Jakirlic's study

in the horizontal midplane. Figures 24 and 25 suggest that the model did not capture the turbulence properly. However, the boundary condition given for the swirler inlet may have had more of an influence on the inaccurate turbulent stresses. Since the

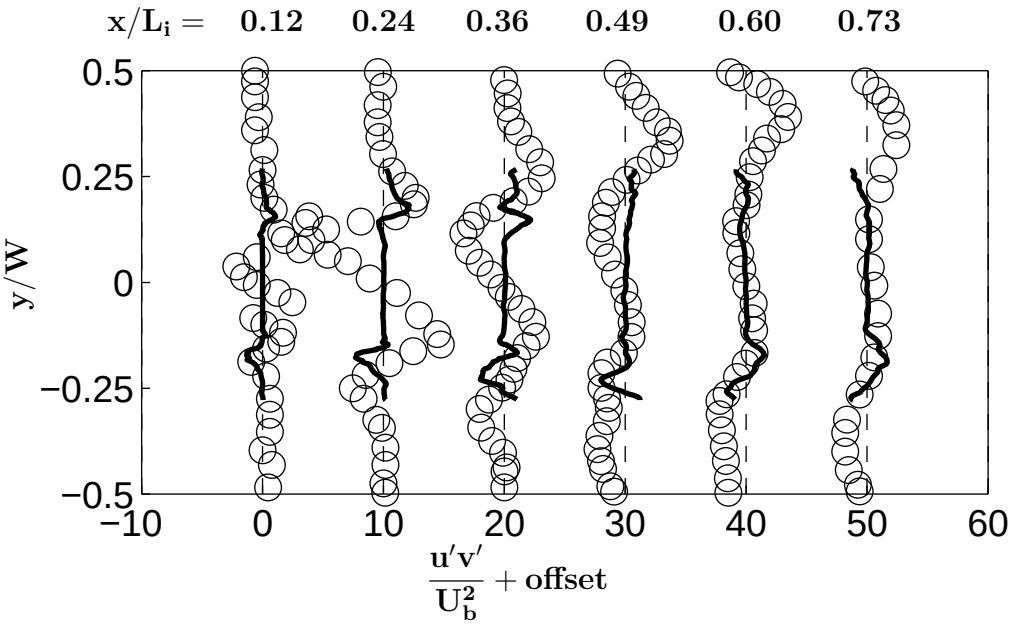


Fig. 25.: Plot of shear stress component profiles and comparison to previous data. The simulation fails to predict the highly turbulent core near the swirler entrance.

simulation results still follow the general trend of the experimental data, then the bulk motion of the fluid has been successfully captured (a major goal of this study). A major reason for the seemingly lack of turbulence in the results is simply that no upstream turbulence was generated. While the swirl imparted on the inlet flow seems to match well with the experimental (and numerical) results from Jakirlic, they had the added benefit of allowing the turbulence in the flow to develop **before** it exits the swirler. Since including the swirler in the geometry provides a significant strain on the computational costs (in terms of added mesh complexity), it was thought that the inlet could be successfully modeled through functions. The results show that this may not be possible, and so adding the swirler to even this simple domain will be a focus in the near future.

Figures 24 and 25 are normalized by their maximum values in Figures 26 and 27 so that everything is scaled to unity. While this is not a fair normalization to make, it allows for at least qualitative comparisons to be made.

Referring to Figures 26 and 27, the turbulence plots normalized to unity give an idea of how the simulation predicts turbulence on a qualitative basis. The simulation's streamwise stress component follows the trends fairly well, but the shear stress component is still different, as some profiles seem to be reversed. In order to validate the present model, these deficiencies will have to be addressed.

## C. Results for $J = 100$ Case

The case with the dilution jets added provided a great stress test for the HPF Smagorinsky model. A major issue that came about in this study was the control of mesh quality. Particularly with spectral elements, it is often better to lose some resolution in a problem area than attempt a refinement that could drastically degrade

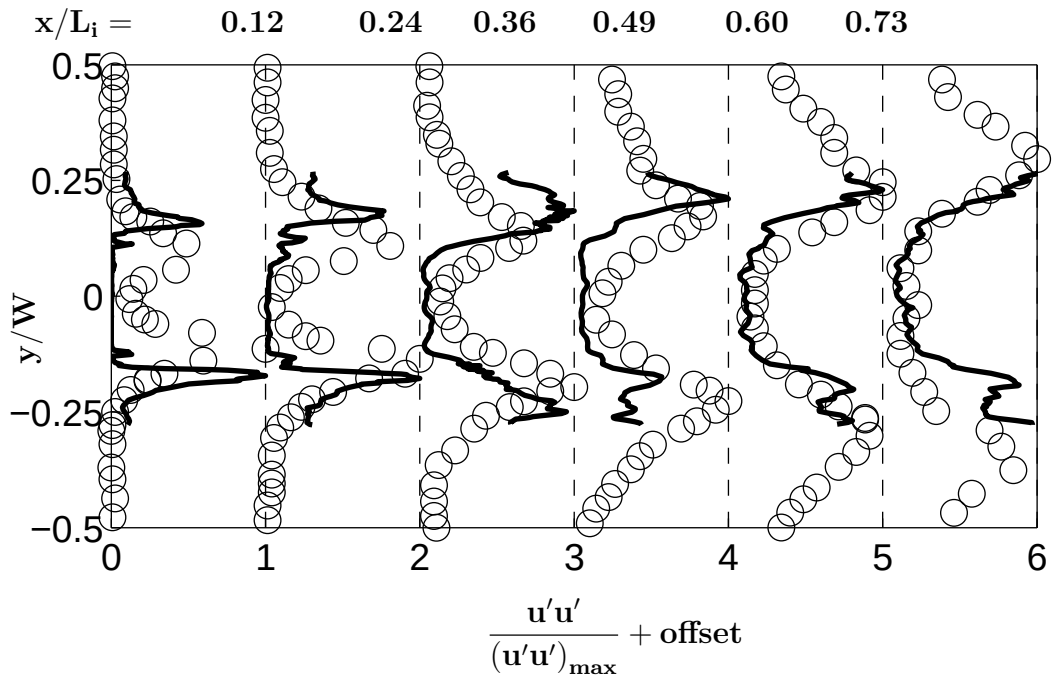


Fig. 26.: Plot of streamwise stress component profiles normalized by magnitudes for $J = 0$. Although only qualitative comparisons can be made here, generally good agreement is seen between the present study and the experiment [15]

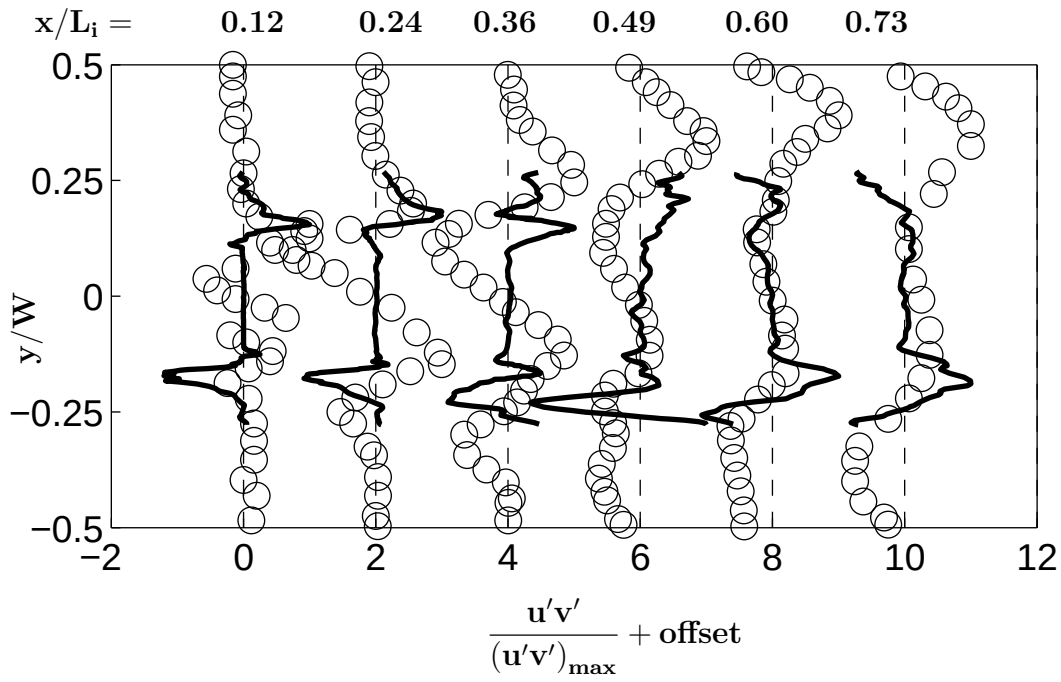


Fig. 27.: Plot of shear stress component profiles normalized by magnitude for $J = 0$ The simulation struggles somewhat to capture the shear stress present in [15] in some areas, even qualitatively, but in other areas it follows it well.

the mesh quality, such as creating highly skewed element. However, if one coarsens in an area of high velocity gradients, then the simulation could become unstable, so a fine balance must be sought. The benefit of using NEK5000 for this study was that a problem area with highly skewed elements could be coarsened, and the the entire domain's polynomial order could be increased to compensate. Although at first glance this appears to make the situation worse, it was found in this study to improve the stability of the simulation considerably, which is to be expected considering that the purpose of LES is to capture these high frequency vortices.

As expected, the bulk flow features, such as the Precessing Vortex Core and the separation bubble near the dilution jets, were captured successfully. Figure 28, like Figure 21 before it, shows the axial velocity profile at several axial locations, instead this time the profile is in the vertical midplane of the combustor. Like the case with no dilution jets, reasonably good agreement is seen between this study and the experimental results, particularly if the different geometries are taken into account. The velocity distribution tends to spread out more quickly in this study. However, no attempts were made to normalize this as in 21, as it is difficult to know the proper way to perform this adjustment.

Figure 29 shows a plot of time averaged streamlines. The influence of the jets on the PVC is clearly seen here. Also, the point where the high velocity air from the swirler hits the combustor is further downstream, and the corner vortex is much larger. Still, the jet of air from the swirl diverges far to quickly when compared to that of Jarkirlic, further implying that the boundary conditions for this simulation must be improved. One can also note a separation bubble immediately downstream of the dilution jets. Overall, the LES model successfully captured all of the large scale features that were expected to be seen.

Unfortunately, as before, the streamwise and shear stresses do not compare well

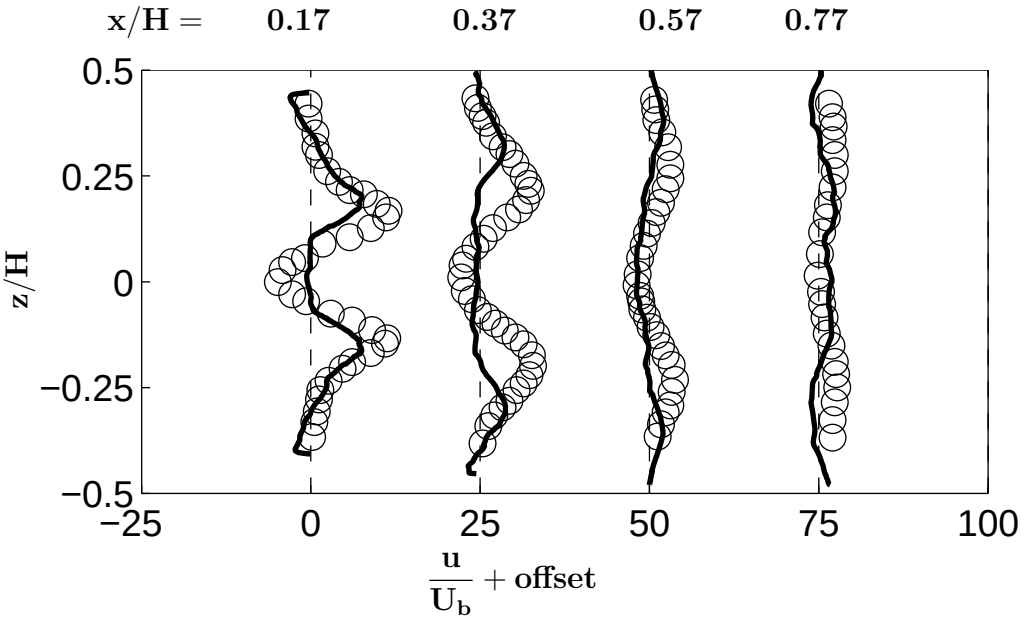


Fig. 28.: Axial velocity profiles in the vertical midplane for the case $J = 100$. Both the axial and wall normal directions are normalized by the height, $H$, of the domain, and the velocities are normalized by the bulk velocity as before. Reasonably good agreement is seen between the experiment [15] and the present study. Note that the dilution holes are located at $x/H = 0.57$

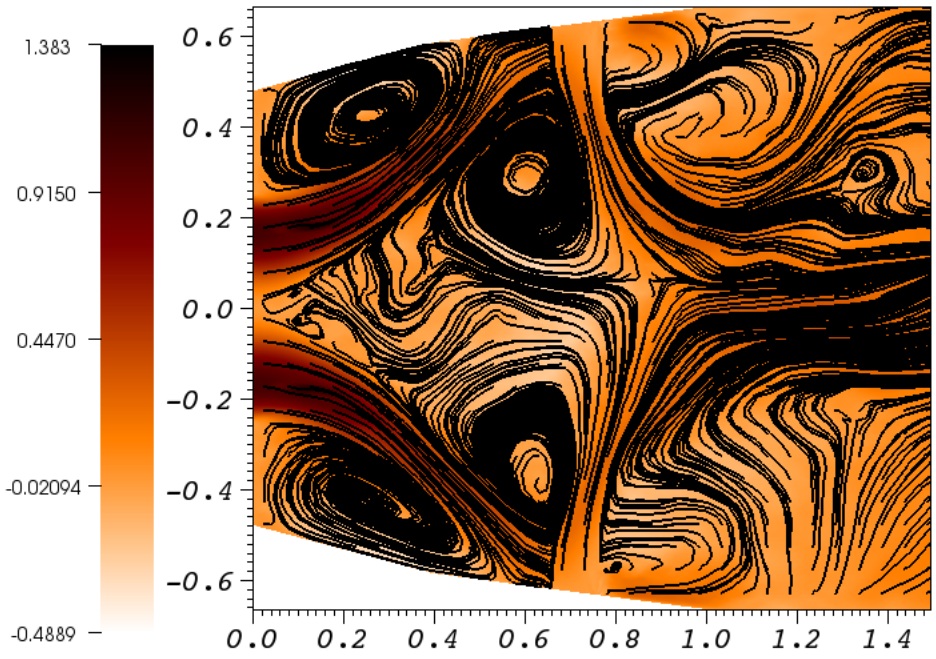


Fig. 29.: Time averaged streamlines and axial velocity contour in vertical midplane for $J = 100$. The data is time-averaged over 3.23 seconds. When compared to the case with no cooling holes (Figure 23), the point at which the air emitting from the jet hits the wall is slightly further downstream, and the high velocity dilution jets cause the strong backflow in the primary zone. Only the first half ($L/2$) of the domain in the axial direction is shown for clarity

to experiment. There swirler inlet is essentially turbulence free, as the velocity is prescribed as a boundary condition instead of coming from a physical swirler, and thus high turbulence levels are not to be expected. As in Figures 26 and 27, the profiles are normalized by the maximum respective stress component in order for qualitative measurements to be made. Figures 30 and 31 show the streamwise and shear stress components compared to Jakirlic, normalized to unity for comparison.

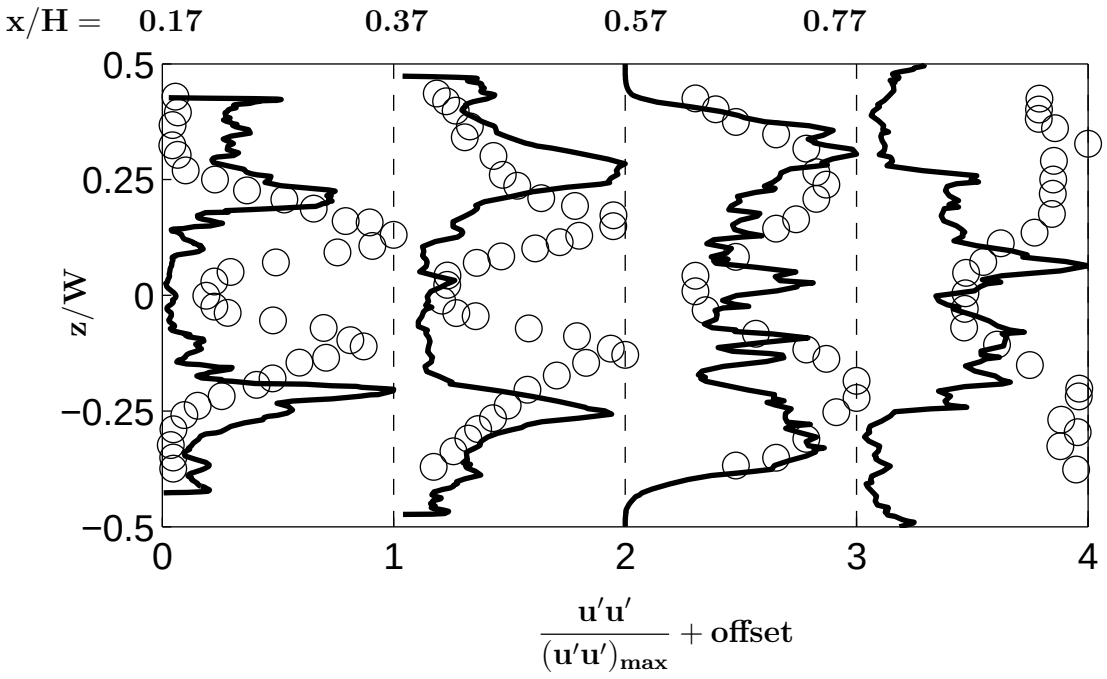


Fig. 30.: Profiles of streamwise stress component along the vertical midplane. When normalized for qualitative comparisons, the agreement between the present study and Jakirlic [15] is reasonably good.

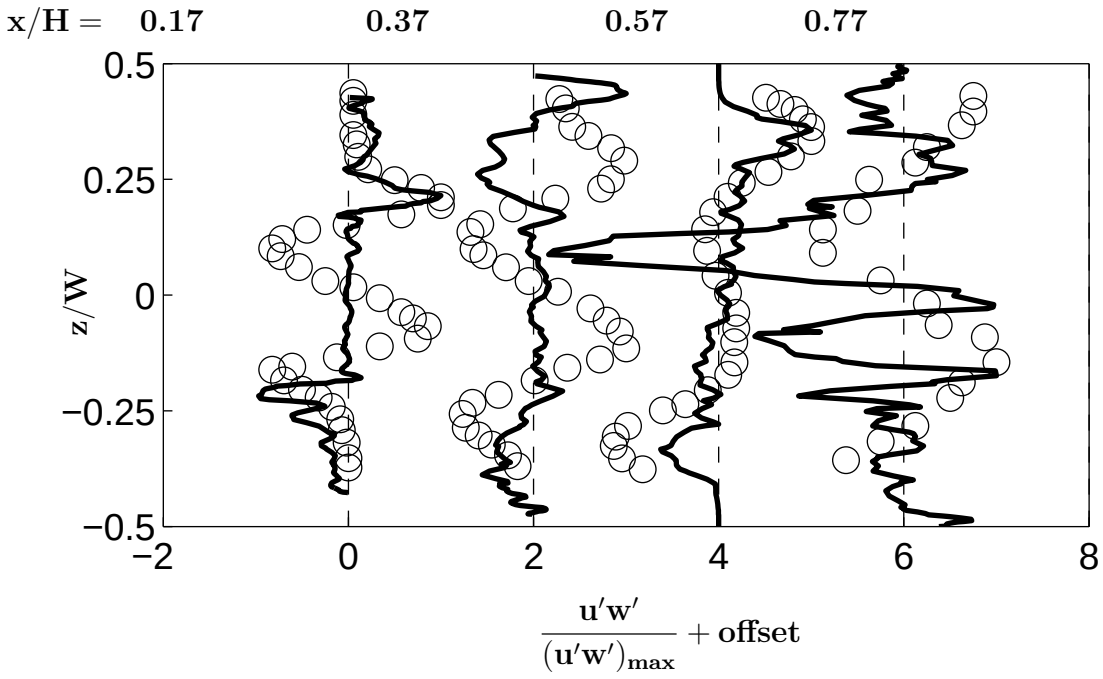


Fig. 31.: Profiles of shear stress component in vertical midplane. Even when normalized, the present data doesn't follow the experimental data [15] exactly.

## D. Future Considerations

There is further work that should be done to complete this study, both presently and towards the future project.

### 1. Current Study

The largest issue is making corrections to the domain, both in terms of geometry and boundary conditions. The domain must be made larger so that the $y$ direction is truly periodic. Also, there are many difficulties in modeling the inlet swirl, with a plethora of different velocity profiles to choose from. Jakirlic did not take the approach of modeling the inlet flow, and instead directly included the swirler itself. The inclusion of the swirl nozzle will be the next step, as well as properly widening the domain, as this should eliminate much of the uncertainty involved with the results obtained. A further step will be to include the turbulence generating recycling plane shown in [20], as this will better emulate the turbulent flow coming from the compressor.

### 2. Future Work

Schwaenen [20] investigated the horseshoe vortex structure that is present at the leading edge of the first stage turbine vane (see Figure 32). This structure greatly enhances the heat transfer to the blade, causing thermal wear and possibly eventual failure. The study used the Walsh solution to the Navier-Stokes equations, along with other turbulence generation techniques, to approximate the flow conditions exiting the combustor. The goal of the future work is to remove the approximated velocity inlet technique for the blade and instead directly attach a combustor domain, resulting in one massive simulation. This will be done in order to study the effects that true combustor exit velocity and temperature profiles have on the horseshoe vortex.

A couple of cases will be looked at: one involving this simple domain (with the improvements mentioned above) and a simple turbine blade domain, and another, more complex combustor coupled with a turbine vane domain with film cooling holes. Figures 33 and 34 show these two domains. Work will also be done to add combustion simulation capabilities to NEK5000. Because of the open source nature of NEK5000, this will open up a whole new avenue for researchers who want to perform combustor simulations.

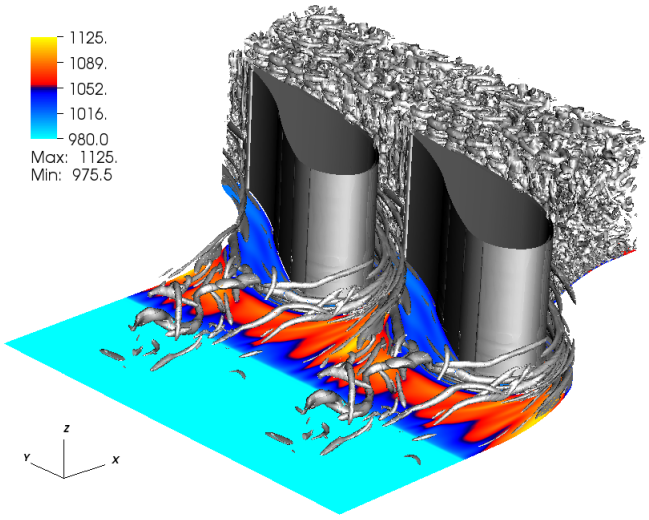


(a) DNS without cooling holes

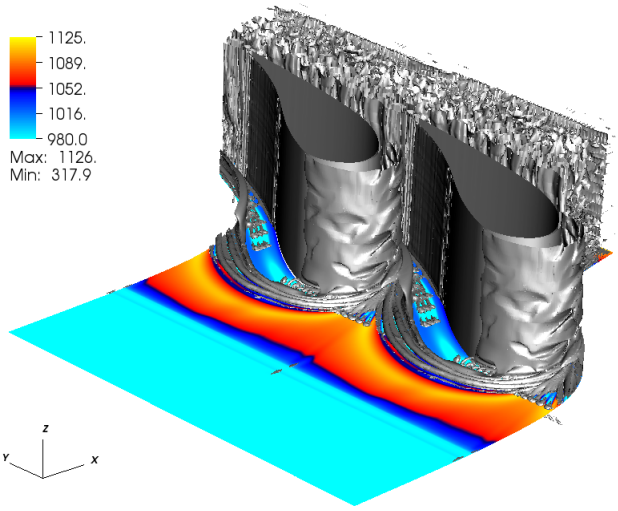


(b) DNS with cooling holes

Fig. 32.: Depiction of horseshoe vortex structures near turbine vane endwall. The vortex structures (gray) have a profound effect on endwall temperature (color contour). These results will be used for comparison to the future study [20].

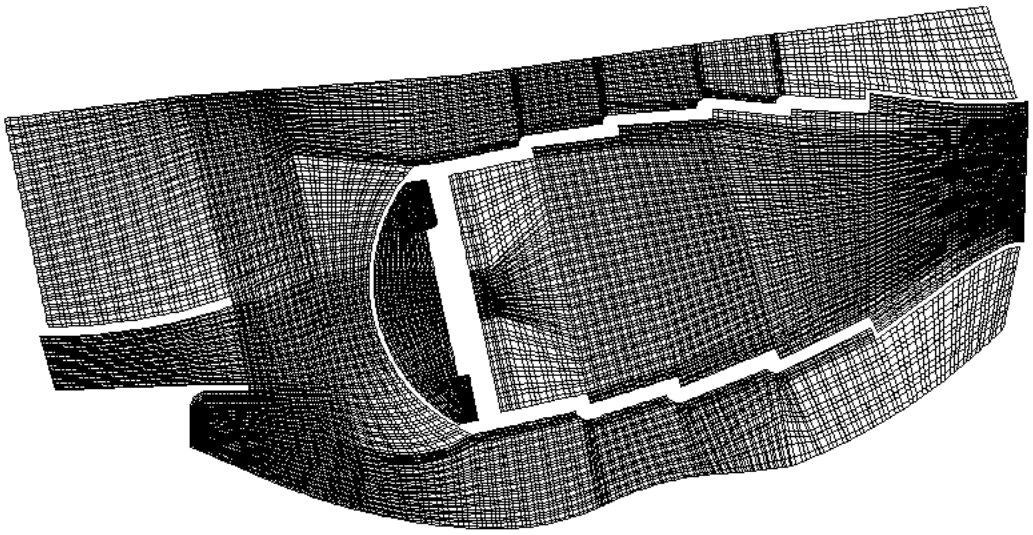

Fig. 33.: Computation domain of model gas turbine combustor. The "coarse" version of this domain consists of over 100,000 elements. Note that the mesh, as shown, is not completed.

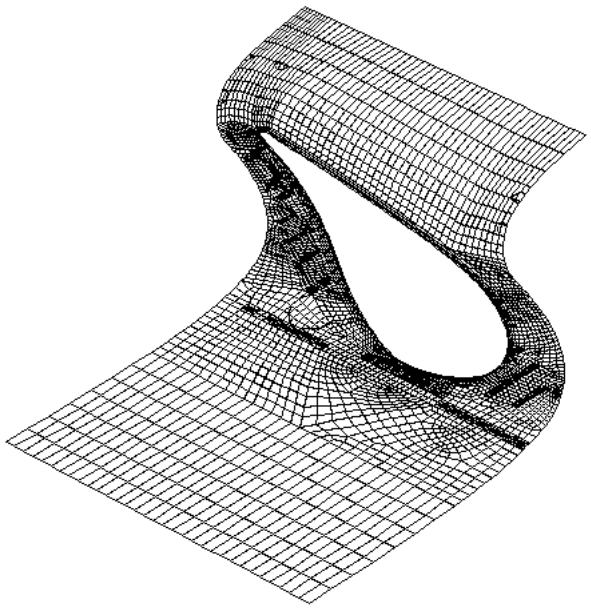

Fig. 34.: Computation domain of first stage turbine vane blade with film cooling holes. This domain was used in [20] with simulated turbulence characteristics at the inflow due to a complex set up upstream (not shown). The future work will combine this with the combustor to study the effects of true combustor exit condition on heat transfer characteristics near the turbine vane.

# CHAPTER IV

## CONCLUSIONS

Gas turbine engines, even in a world searching for alternatives to fossil fuels, still play a large role in the power generation of today's society. Therefore, it is pertinent that these machines continue to improve, both in terms of power as well as efficiency, as even the smallest increases can have a large impact in terms of both economics and energy conservation.

To make these improvements, designers need accurate and plentiful data. Whereas a large amount of work has been done on turbine blades, both experimentally and computationally, the combustor remains an area that is lacking in data. Experimentally obtained results for flow dynamics are hard to come by because of the geometry and harsh temperature environment of a typical gas combustor. Detailed numerical results are also rare because of the large computational requirement for DNS, and the unsteadiness of the flow inside the chamber make a typical RANS simulation unsuitable. Large eddy simulations provide a reasonable balance between the accuracy of DNS and the ease of RANS, and together with the rapid advancement of supercomputing, LES is an ideal choice for simulation of the gas turbine combustor.

A future study will combine a realistic model of a gas turbine combustor with the flow domain of over the first stage turbine vane. The goal is to understand how true combustor exit conditions affect the secondary flows present on the endwall of the turbine section using a large eddy simulation. First, the proposed model, along with the high order spectral element solver used, was compared with previous experimental results [15]. The case with no dilution flow performed well in capturing important bulk movements, such as the Precessing Vortex Core, but it failed to accurately predict turbulent quantities. However, this was shown to be more of a problem with

geometry differences, as well as difficulties in mathematically modeling the inlet flow from the swirler.

The case with dilution holes added struggled with stability issues due to the combination of poor meshing quality and high velocity gradients near the dilution jets. However, once past these trouble points, the simulation predicted bulk movements fairly well, and painted a good picture of what the flow inside the combustor looks like. This simulation provided a great stress test for NEK5000, as it featured reasonably complicated geometries and flow conditions.

The dilution hole case will be run for some more time to ensure it is at a statistically steady state, and then have its solution compared to Jakirlic again. As a further test of NEK5000's ability to resolve domains with highly turbulent, swirling flows and complex geometries, a case will be run on the domain used by Jakirlic. This will provide the validation needed to pursue study of more complicated combustors, both in terms of the physical model used and the geometry.

# REFERENCES

[1] Rolls Royce plc, *The Jet Engine*, London, England: Rolls Royce, 2005.

[2] M. Schobeiri, *Turbomachinery Flow Physics and Dynamic Performance*, New York: Springer, 2005.

[3] J. C. Han, S. Dutta, and S. V. Ekkad, *Gas Turbine Heat Transfer and Cooling Technology*, New York: Taylor & Francis, 2000.

[4] S. B. Pope, *Turbulent Flows*, New York: Cambridge University Press, 2000.

[5] R. J. Goldstein, *Fluid Mechanics Measurements, 2nd ed.*, Philadelphia, PA: Taylor & Francis, 1996.

[6] Y. Oyanagi, "Future of supercomputing," *Journal of Computational and Applied Mathematics*, vol. 149, no. 1, pp. 147 – 153, 2002.

[7] A. Shanley, "Pushing the limits of cfd: Research and new software are extending cfd's reach," *Chemical Engineering*, vol. 103, no. 12, pp. 66, 1996.

[8] M. V. Heitor and J. H. Whitelaw, "Velocity, temperature, and species characteristics of the flow in a gas-turbine combustor," *Combustion and Flame*, vol. 64, no. 1, pp. 1 – 32, 1986.

[9] J. J. McGuirk and J. M. L. M. Palma, "Experimental investigation of the flow inside a water model of a gas turbine combustor: Part 1—mean and turbulent flowfield," *Journal of Fluids Engineering*, vol. 117, no. 3, pp. 450–458, 1995.

[10] P. Koutmos and J. J. McGuirk, "Isothermal modeling of gas turbine combustors: Computational study," *Journal of Propulsion and Power*, vol. 7, no. 6, pp. 1064 – 1071, 1991.

[11] K. Menzies, "Large eddy simulation applications in gas turbines," *Phil. Trans. R. Society A.*, vol. 367, pp. 2827–2838, July 2009.

[12] F. di Mare, W. P. Jones, and K. R. Menzies, "Large eddy simulation of a model gas turbine combustor," *Combustion and Flame*, vol. 137, no. 3, pp. 278 – 294, 2004.

[13] K. Mahesh, G. Constantinescu, S. Apte, G. Iaccarino, F. Ham, and P. Moin, "Large-eddy simulation of reacting turbulent flows in complex geometries," *Journal of Applied Mechanics*, vol. 73, no. 3, pp. 374–381, 2006.

[14] W. Kim, S. Menon, and H. Mongia, "Large-eddy simulation of a gas turbine combustor flow," *Combustion Science and Technology*, vol. 143, pp. 25–62, 1999.

[15] S. Jakirlic, B. Kniesner, G. Kadavelil, M. Gnirß, and C. Tropea, "Experimental and computational investigations of flow and mixing in a single-annular combustor configuration," *Flow, Turbulence and Combustion*, vol. 83, pp. 425–448.

[16] G. Staffelbach, J. Senoner, L. Gicquel, and T. Poinsot, "Large eddy simulation of combustion on massively parallel machines," in *High Performance Computing for Computational Science - VECPAR 2008*, J. Palma, P. Amestoy, M. Dayd, M. Mattoso, and J. Lopes, Eds., vol. 5336 of *Lecture Notes in Computer Science*, pp. 444–464. Berlin: Springer, 2008.

[17] P. F. Fischer, J. W. Lottes, and S. G. Kerkemeier, "nek5000 Web page," 2008 [Retrieved May 2011], http://nek5000.mcs.anl.gov.

[18] L. C. Berselli, T. Iliescu, and W. J. Layton, *Mathematics of Large Eddy Simulation of Turbulent Flows*, New York: Springer, 2006.

[19] S. Stolz, P. Schlatter, and L. Kleiser, "High-pass filtered eddy-viscosity models for large-eddy simulations of transitional and turbulent flow.," *Physics of Fluids*, vol. 17, no. 6, pp. 065103, 2005.

[20] M. Schwänen, M. Meador, J. Camp, S. Jagannathan, and A. Duggleby, "Massively-parallel direct numerical and large eddy simulations of turbine vane endwall horseshoe vortex dynamics and heat transfer," *ASME Paper GT2011-45915*, 2011.

[21] L. C. Deville, P. F. Fischer, and E. H. Mund, *High-Order Methods for Incompressible Fluid Flow*, New York: Cambridge University Press, 2002.

[22] OpenCFD Limited, "Openfoam website," 2011 [Retrieved May 2011], http://www.openfoam.com/.

[23] M. A. Sprague, "A comparison of nek5000 and openfoam for dns of turbulent channel flow," presented at the 2010 NEK5000 Users Meeting in Argonne, IL, December 2010.

# VITA

Joshua Lane Camp received his Bachelor of Science degree in Mechanical Engineering from Baylor University in 2009. He entered Professor Andrew Duggleby's research group at Texas A&M University in 2009 and began research into numerical experiments of complex geometries. He graduated from Texas A&M with a Master of Science in Mechanical Engineering in May of 2011, and will pursue a PhD in Mechanical Engineering in the Fall of 2011 at Texas A&M as well. His research interests are in high order CFD of complex geometries as well as general mesh generation techniques that will simplify the numerical process.

Joshua may be reached at 3123 TAMU, College Station, TX 77843-3123 or at josh.camp@tamu.edu.

The typist for this thesis was Joshua Lane Camp.